

# Boundary-layer transition by interaction of discrete and continuous modes

YANG LIU<sup>1</sup>, TAMER A. ZAKI<sup>2</sup> AND PAUL A. DURBIN<sup>3</sup>

<sup>1</sup>Mechanical Engineering, Stanford University, CA 94305, USA

<sup>2</sup>Mechanical Engineering, Imperial College London, SW7 2AZ, UK

<sup>3</sup>Aerospace Engineering, Iowa State University, IA 50011, USA

(Received 31 July 2007 and in revised form 19 February 2008)

The natural and bypass routes to boundary-layer turbulence have traditionally been studied independently. In certain flow regimes, both transition mechanisms might coexist, and, if so, can interact. A nonlinear interaction of discrete and continuous Orr–Sommerfeld modes, which are at the origin of orderly and bypass transition, respectively, is found. It causes breakdown to turbulence, even though neither mode alone is sufficient. Direct numerical simulations of the interaction shows that breakdown occurs through a pattern of  $\Lambda$ -structures, similar to the secondary instability of Tollmien–Schlichting waves. However, the streaks produced by the Orr–Sommerfeld continuous mode set the spanwise length scale, which is much smaller than that of the secondary instability of Tollmien–Schlichting waves. Floquet analysis explains some of the features seen in the simulations as a competition between destabilizing and stabilizing interactions between finite-amplitude distortions.

---

## 1. Introduction

The notion that boundary-layer transition can proceed either via, or in the absence of Tollmien–Schlichting(T-S) instability waves has existed since the advent of Orr–Sommerfeld(O-S) theory. The failure to detect T-S waves in experiments led Taylor (1936) to postulate what today is called a ‘bypass’ mechanism. Once T-S waves were discovered in the laboratory, they became the subject of an enormous amount of research. Nevertheless, it remained true that very low levels of free-stream turbulence were required if T-S waves were to be seen in the laboratory. Our current understanding is that when free-stream turbulence intensity exceeds 1% of the mean velocity, T-S waves are bypassed. Nevertheless, there may be a role for T-S waves even in the presence of free-stream vortical disturbances. We explore that herein.

### 1.1. Natural transition

The focus of orderly, or natural, transition research has been the amplification of primary T-S waves, and their secondary instability which precedes breakdown to turbulence (Herbert 1988). In zero-pressure-gradient boundary layers, the first unstable mode is two-dimensional and occurs at a critical Reynolds number,  $Re \equiv \sqrt{Ux}/\nu \approx 270$ , or based on the momentum thickness,  $Re_\theta \approx 201$ . Beyond the critical Reynolds number, transition to turbulence is not inevitable; amplifying T-S waves can return to a stable state if they cross the upper branch of the neutral stability curve. If, however, unstable T-S waves reach nearly 1% of the free-stream velocity, they develop three-dimensional instabilities.

Secondary instability theory (Herbert 1983) attributes these three-dimensional disturbances to parametric excitation of the new base flow, which consists of the Blasius profile plus a saturated T-S wave that is periodic in the streamwise direction. The secondary instability modes provide an explanation of the  $\Lambda$ -patterns which precede breakdown, and which were first observed in experiments by Klebanoff, Tidstrom & Sargent (1962). Subsequent rows of emerging  $\Lambda$ -structures can be aligned or staggered depending on the flow conditions. Aligned  $\Lambda$ -structures (K-type) are the result of fundamental resonance, whereas the staggered arrangements (called C-type and H-type) are the result of subharmonic resonance. The amplification of secondary instabilities is followed by breakdown of the  $\Lambda$ -structures in regions of elevated shear. The breakdown process continues downstream forming smaller structures and, finally, a fully turbulent boundary layer (Kleiser & Zang 1991).

### 1.2. Bypass transition

Often, the proceedings of natural transition are either entirely absent or are difficult to identify within the transitional region of the flow. These instances of boundary-layer breakdown have become collectively and indiscriminately known as bypass transition. Bypass is therefore a reference to what the mechanism is not. The term bypass has, however, become synonymous with transition due to free-stream vortical perturbations. Even for this class, variations occur according to the flow conditions; for example the leading-edge geometry (Kendall 1991) and the mean pressure gradient and its history (Abu-Ghannam & Shaw 1980; Gostelow, Blunden & Walker 1994). Even experiments with seemingly similar conditions report different transition onset and extent, depending on the free-stream turbulence characteristics, such as the level of anisotropy and decay rate (Westin *et al.* 1994).

In the absence of leading-edge effects and streamwise pressure gradient, bypass transition due to free-stream turbulence,  $Tu \geq 1\%$ , takes place without the mediation of T-S instability waves. Instead, transition is preceded by the formation of large-amplitude elongated disturbances, termed Klebanoff modes (Kendall 1985). Their instantaneous appearance resembles ‘streaks’, or jets, in the perturbation field. The wall-normal and spanwise velocities of the perturbations remain of the order of the free-stream  $Tu$ , while the streamwise component grows to the order of 10–20% of the mean free-stream velocity, giving them a jet-like character.

Klebanoff modes have received a great deal of attention in the literature. Experimental investigations have documented their spatial amplification, dependence on the turbulence intensity, and the ‘universality’ of the disturbance wall-normal profile (see for e.g. Westin *et al.* 1994; Matsubara & Alfredsson 2001). Their long wavelength, in comparison to the free-stream disturbance spectrum, has been explained by the filtering effect of the mean shear (Hunt & Durbin 1999). These elongated disturbances are created from isotropic free-stream turbulence because only low-frequency vortical perturbations can penetrate the boundary-layer shear. The physical mechanism for growth of these distortions is lift up, or displacement, of mean momentum (Phillips 1969). Various mathematical formulations of this process have been proposed, deriving from non-modal growth analyses (Butler & Farrell 1992; Andersson, Berggren & Henningson 1999; Luchini 2000), or from the solution of the initial-value problem of the Squire response to O-S mode forcing (Zaki & Durbin 2005, 2006). Though the amplification of Klebanoff streaks has been well studied, their influence in bypass transition remains less understood.

Direct numerical simulations (DNS) have provided a detailed empirical view of the interaction of free-stream turbulence with boundary layers. Jacobs & Durbin (2000)

carried out simulations in zero pressure gradient, and in the absence of leading-edge effects. They synthesized free-stream turbulence from the continuous spectrum modes of the O-S equation; these modes are the complement to discrete T-S waves in O-S theory. The instantaneous fields from the DNS captured the amplification of the low-frequency streaks, their secondary instability due to high-frequency forcing from the turbulent free stream, and finally the inception of turbulent spots.

In order to isolate the influence of particular spectral components of the free-stream perturbation, Zaki & Durbin (2005, 2006) carried out simulations of continuous mode transition. In these basic studies, two continuous modes were prescribed at the inlet, and their interaction and breakdown are computed using DNS. It was found that the main features of transition under free-stream turbulence can be emulated by bi-modal interactions.

In zero pressure gradient, T-S waves have a small exponential growth rate. They are not seen under free-stream turbulence of about 1%. However, the term bypass does not preclude the presence of T-S waves entirely. Kendall (1991) demonstrated that amplification of T-S waves became more pronounced as the aspect ratio of his elliptic leading-edge was reduced, while Klebanoff modes were insensitive to the leading-edge geometry. Similarly, in adverse pressure gradient, T-S waves become inviscidly unstable and the critical Reynolds number is reduced. As a result of their increased exponential growth rate, they might reappear within the transitional region of the flow and contribute to breakdown.

### 1.3. Motivation

When both boundary-layer streaks and T-S waves are present, their interaction can be stabilizing or destabilizing. For instance, Cossu & Brandt (2004) and Fransson *et al.* (2005, 2006) studied the interaction between steady streaks and T-S waves. Both the secondary instability analysis and experiments confirmed that steady streaks are stabilizing, and suppress transition. When the streaks are unsteady, the outcome is more curious. Boiko *et al.* (1994) studied this case in the laboratory. Two-dimensional T-S waves were created by a vibrating ribbon beneath grid turbulence of about 1% intensity. Adding T-S waves to the boundary layer caused transition at a lower Reynolds number than under pure free-stream turbulence. That may not seem surprising. However, the free-stream turbulence was observed to reduce the growth rate of T-S waves: free-stream turbulence reduces their growth rate, but nevertheless T-S waves promote transition.

In a less clear cut, but still intriguing study, Hughes & Walker (2001) used wavelet transforms to extract instability waves from within surface stress measurements on the suction surface of a compressor blade. The blade was a stator, downstream of the rotor of a  $1\frac{1}{2}$  stage low-speed cascade. Hence, this is a case of transition induced by impinging wakes. Hughes & Walker (2001) found evidence of growing instability waves in high-pass-filtered data, and asserted that instability waves could always be found prior to the appearance of turbulent spots.

Nagarajan, Lele & Ferziger (2007) performed simulations of turbulence incident on a plate with a blunt leading edge, for two leading-edge aspect ratios. For the smaller aspect ratio, he observed instability wave packets in the streaky boundary layer, upstream of transition. While the packet was related to receptivity at the leading edge, it could not be attributed to discrete instability modes. The noisy perturbation environment inside the boundary layer owing to forcing by free-stream turbulence prevented a clear discernment of the breakdown mechanism. It might conceivably have involved an interaction of T-S and continuous O-S waves.

In this paper, we study the interaction of T-S waves and boundary-layer streaks by numerical simulation. The inlet perturbation is a pair of O-S modes: an unstable T-S wave and a continuous mode. The T-S wave replaces the spectrum of discrete instability waves which would emerge in the presence of a leading edge or other receptivity site, and the continuous mode replaces free-stream turbulence. These conditions deviate from practical configurations, but the fundamental approach provides insight into breakdown. By studying particular disturbances, the boundary layer remains uncluttered upstream of transition, and the breakdown mechanism is easier to identify. Our approach is therefore similar to experimental investigations where a particular T-S wave is forced by a vibrating ribbon, and streaks are introduced by spanwise spacers inside the boundary layer. This approach is well suited to tackling an apparent controversy in the literature regarding the outcome of the interaction of T-S waves and streaks: some experiments suggest that streaks enhance breakdown in natural transition (Kendall 1998; Boiko *et al.* 1994), while other experiments indicate that forced T-S waves are less amplified in the presence of streaks, and transition can be delayed (Fransson *et al.* 2005).

This paper is divided into five sections. The numerical method and grid resolution tests are summarized in §2. The DNS reproduce the seemingly contradictory observations from the literature: streaks reduce the amplification of T-S waves, but their influence on transition location is parameter dependent: they can either accelerate the secondary instability and breakdown (§3) or delay this process (§4). The choice of the continuous mode also affects the pattern of the secondary instability of T-S waves. An informal explanation for the strong interaction of discrete and continuous modes is provided by Floquet analysis in §5.

## 2. The numerical model

Direct numerical simulations (DNS) with the full Navier–Stokes equations are employed to study the nonlinear modal interactions. The numerics need not be described at length, as the computer code has been used in previous studies (Wu *et al.* 1999; Zaki & Durbin 2005, 2006) and is described elsewhere. The numerical method is a fractional step algorithm for the time-dependent three-dimensional incompressible Navier–Stokes equations in generalized coordinate systems, developed by Rosenfeld, Kwak & Vinokur (1991). The governing equations are discretized by finite volumes on a staggered mesh. The spanwise direction is assumed to be periodic and is treated by spectral methods to reduce computational cost. The convective terms and the off-diagonal diffusion terms are advanced explicitly by the Adams–Bashforth scheme, whereas the remaining diffusion terms are treated implicitly by Crank–Nicolson. Finally, the Poisson equation for pressure is solved by a multi-grid algorithm. This code is MPI parallel and the simulations were performed on 32 processors of an Opteron 280 cluster.

The computational set-up is illustrated in figure 1. Based on the local boundary-layer thickness, the inlet plane Reynolds number is  $Re_{\delta_{99}}(x_0) \approx 2000$ . The streamwise extent of the domain is  $L_x = 200\delta_{99}$ , its height  $20\delta_{99}$ , and its spanwise extent  $L_z = 8\delta_{99}$ . In terms of the Blasius length scale,  $Re \equiv \sqrt{Ux}/\nu$ , the computational domain spans  $400 \leq Re \leq 750$ . The inflow plane is, therefore, downstream of the critical value,  $Re_c \sim 270$ , and the outflow plane is well below the transition Reynolds number,  $Re_{tr} \sim 1800$  for full breakdown via the Tollmien–Schlichting route. Nonetheless, the domain is sufficiently long for us to investigate bypass mechanisms, where a fully

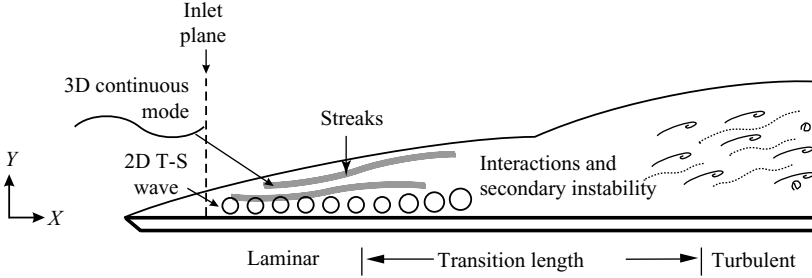


FIGURE 1. Schematic of the discrete-continuous mode interaction. The dashed line marks the boundaries of the computational domain.

turbulent boundary layer can be reached at  $Re \sim 550$  (Jacobs & Durbin 2000; Zaki & Durbin 2005, 2006).

In the simulations, no-slip boundary conditions are enforced at the bottom wall and the the upper boundary is a slip surface. The domain height is 20 inlet boundary-layer thicknesses. It is therefore sufficiently large and the upper boundary slip condition does not significantly affect the evolution of the boundary layer. A convective outflow condition is applied at the exit of the flow domain.

The inflow condition is a superposition of a spatial three-dimensional continuous mode  $(\hat{u}_{con}, \hat{v}_{con}, \hat{w}_{con})$  and a spatial two-dimensional T-S wave  $(\hat{u}_{TS}, \hat{v}_{TS}, 0)$  onto a Blasius mean flow  $(U_b, V_b, 0)$ .

$$u_0 = U_b + \text{Re}(A_{con} \hat{u}_{con} e^{i(k_z z - \omega_{ost} t)} + A_{TS} \hat{u}_{TS} e^{-i\omega_{TS} t}) \quad (2.1a)$$

$$v_0 = V_b + \text{Re}(A_{con} \hat{v}_{con} e^{i(k_z z - \omega_{ost} t)} + A_{TS} \hat{v}_{TS} e^{-i\omega_{TS} t}) \quad (2.1b)$$

$$w_0 = \text{Re}(A_{con} \hat{w}_{con} e^{i(k_z z - \omega_{ost} t)}) \quad (2.1c)$$

The T-S and continuous modes are obtained by solving the O-S and Squire equations by well-established methods: a Chebyshev collocation scheme is used to find the discrete modes and an implicit matrix method is used for the continuous modes.

### 2.1. Single-mode simulations

In all the simulations, the inflow T-S wave has a non-dimensional frequency

$$F \equiv \frac{\omega v}{U_\infty^2} 10^6 = 124.$$

The mode shape, which is superposed onto the Blasius mean flow, is shown in figure 2. At the inlet Reynolds number, the mode is unstable and has a complex wavenumber

$$\alpha \delta_{99} = 0.6643 - 3.355 \times 10^{-3} i. \quad (2.2)$$

This mode is stable at the outflow Reynolds number. The inflow and outflow states are identified on the neutral curve in figure 3(a). When prescribed alone at the inlet to the computational domain, the discrete mode initially amplifies downstream, and subsequently decays upon crossing the upper branch of the neutral stability curve. The downstream amplification computed from DNS is shown in figure 3(b). The wall-normal maximum in the root mean square and instantaneous  $u$ -perturbations are both shown. The figure shows the onset of modal decay near  $Re \approx 625$ , which is consistent with the neutral stability curve.

Owing to the near-wall peak in their mode shape, amplifying T-S waves significantly modify the instantaneous skin friction curve. Figure 4 shows the skin friction

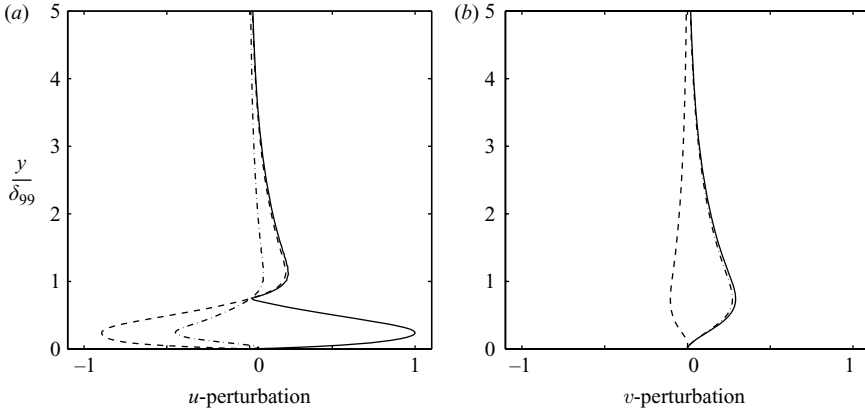


FIGURE 2. Profile of the T-S mode. The (a)  $u$ -component, and (b) the  $v$ -component. —, mode amplitude; - - -, real part; —·—, imaginary part.

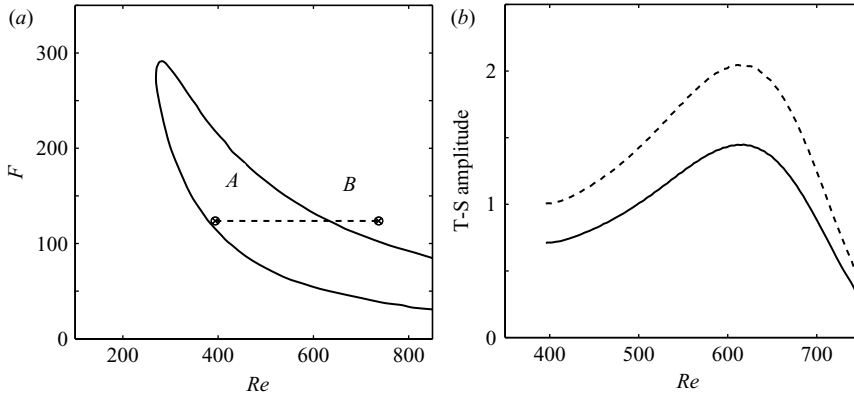


FIGURE 3. (a) The neutral curve for a zero-pressure gradient boundary layer (Bertolotti, Herbert & Spalart 1992).  $A$  and  $B$  mark the inlet and exit conditions for the T-S wave. (b) The downstream evolution of the  $u$ -perturbation. —,  $\max(u_{rms}(y))$ ; - - -,  $\max(u(y, t)) = \sqrt{2}\max(u_{rms})$ .

coefficient of the boundary layer under T-S waves in comparison to the theoretical curves for laminar and turbulent boundary layers. The amplified instability wave does not, however, develop any secondary instabilities within the computation domain, and the boundary layer remains laminar.

The inflow continuous O-S modes used in this study are adapted from Zaki & Durbin (2005, 2006). Their non-dimensional frequency, wall-normal and spanwise wavenumbers are, respectively,

$$F = 33, \quad k_y \delta_{99} = \pi/2, \quad k_z \delta_{99} = n2\pi/L_z = nk_z^0, \quad (2.3)$$

in which

$$k_z^0 = \frac{2\pi}{L_z} = \frac{2\pi}{8\delta_{99}}; \quad (2.4)$$

this is the wavenumber with period equal to the domain width. These modes will, hereinafter, be designated according to the integer  $n$  which determines their spanwise

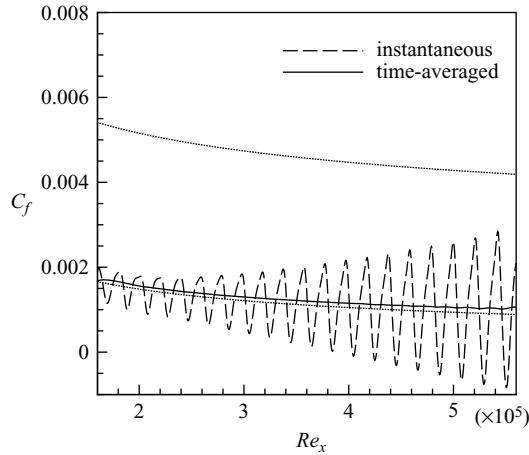


FIGURE 4. The skin friction coefficient vs. the  $Re_x$ ;  $t = 3\tau$ . - - -, instantaneous; —, time averaged (Blasius is shown by dotted line); ..., turbulent.

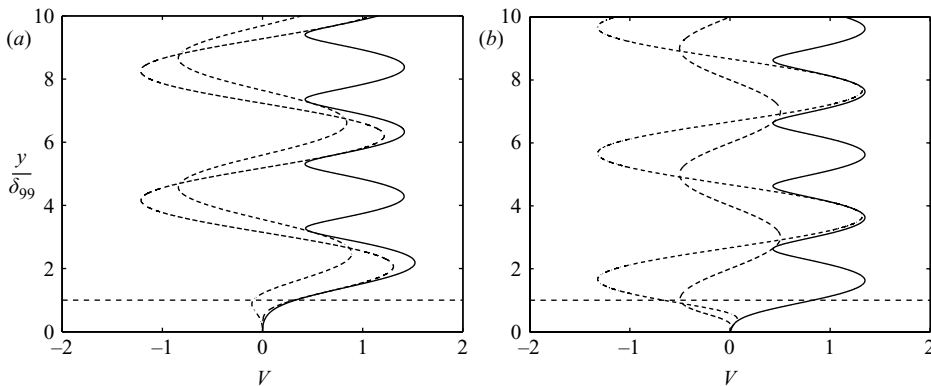


FIGURE 5. Profiles of (a)  $v$  and (b)  $\eta$  for mode 2. —·—, real; - - -, imaginary; —, ABS.

wavenumber, for example mode 2 has  $k_z = 2k_z^0$  and therefore a wavelength equal to  $4\delta_{99}$ . To a good approximation  $\alpha\delta_{99} = \omega\delta_{99}/U_\infty$  for continuous modes. Hence, based on (2.2) and (2.3), the streamwise wavelength of the continuous mode is about 10 times the T-S wavelength in our simulations.

Various inlet continuous modes were considered in our study. The outcome of their interaction with T-S waves is exemplified by the influence of modes 2 and 5. Prior to investigating the modal interaction between the continuous and T-S waves, simulations of modes 2 and 5 alone are carried out. The shape of the continuous mode 2 is shown in figure 5; mode 5 possesses a similar profile since it shares the same frequency and wall-normal wavenumber, and both parameters determine the extent of mode penetration into the boundary layer. The two modes, however, differ in spanwise wavenumber. As a result, the boundary-layer response to each of these three-dimensional inlet disturbances differs. A top view of the perturbation field inside the boundary layer is shown in figure 6. Figure 6(a) is the response due to mode 2, and figure 6(b) to mode 5. Contours of the velocity perturbations clearly show the induced streaks. The streaks initially amplify downstream of the inlet

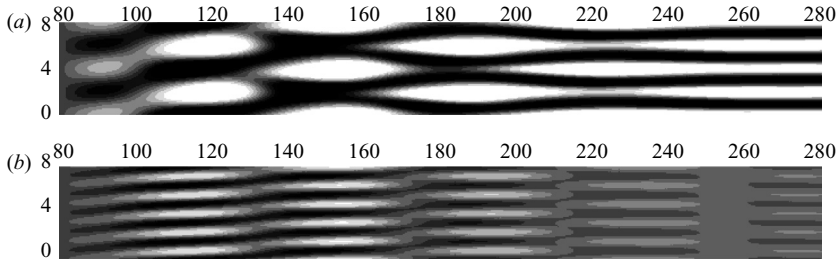


FIGURE 6. Contours of the streamwise velocity perturbation inside the boundary layer owing to inflow perturbation by (a) mode 2 and (b) mode 5;  $t = 3\tau$ ;  $y = 0.5\delta_{99}$ . The spanwise coordinate is enlarged by a factor of 3. Contours are plotted in  $-0.2 < u < 0.2$ .

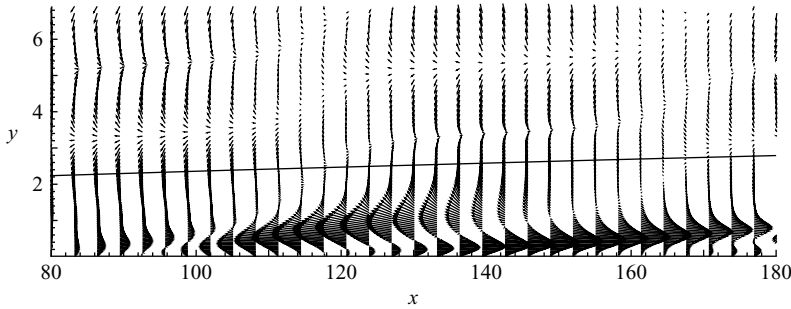


FIGURE 7. The disturbance vector of mode 2 alone;  $t = 3\tau$ .

and subsequently decay, without any symptoms of secondary instability or potential breakdown. The amplitude of the induced streaks is weaker in the case of mode 5, owing to higher viscous dissipation. The streamwise wavelength of the streaks is, in fact, growing for mode 2.

A side view of the perturbation streaks is shown in figure 7 for mode 2. The figure emphasizes the upstream region,  $80 < x < 125$ . The boundary-layer perturbation is dominated by the streamwise velocity component,  $u'$ , and takes the form of forward and backward jets, or streaks. Figure 8 shows the skin friction. Despite the large amplitude of the streaks, the skin friction curve follows the laminar values because  $C_f$  is averaged in the span; the instantaneous  $C_f$  would show spanwise oscillations.

## 2.2. Mode identification

In nonlinear simulations of mode interactions, a spectrum of perturbations emerges downstream of the inlet plane, even when the inlet perturbation is composed of only two modes. In the context of continuous–discrete mode interactions, it is not straightforward to infer the role of boundary-layer streaks on the amplification of a particular T-S wave. Therefore, a method is required to identify the spectral makeup of the perturbation field at various downstream locations.

One approach is to decompose the perturbation field at every downstream location in terms of the O-S and Squire eigenmodes using the bi-orthogonality of the eigenvalue problem (Salwen & Grosch 1981; Tumin 2003). Jacobs (2000) applied this decomposition to DNS data, but found it to be far less informative than Fourier decomposition. As disturbances evolve, they depart significantly from the mode shapes specified at the inlet. Boundary-layer streaks due to a single inlet continuous mode are composed of a spectrum of perturbations, all sharing the same frequency and

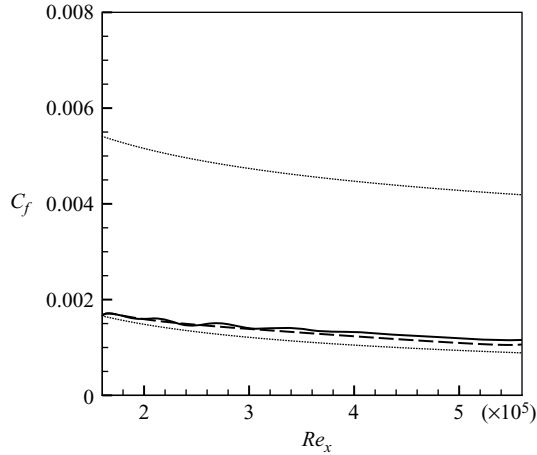


FIGURE 8. The skin friction coefficient *vs.* the  $Re_x$ ;  $t = 3\tau$ . —, instantaneous; - - -, time averaged; . . . , turbulent.

spanwise wavenumber, but each with a different wall-normal wavenumber (Zaki & Durbin 2005, 2006). The  $y$ -profile is not that of pure O-S modes. For present purposes, the perturbation frequency spectra are computed via the Fourier transform of time history. Although this is not a decomposition into O-S modes, we will cite the evolution of Fourier modal energy as evidence of T-S wave evolution.

In the context of secondary instability of T-S waves, the primary interest is the amplification of the fundamental frequency  $\omega$ , its subharmonic  $\omega/2$ , and its first harmonic  $2\omega$ . The modal amplitude at a selected frequency  $\omega$  can be calculated according to

$$\hat{\phi}(\omega) = \sum_{n=1}^{kN} \phi(nT/N) e^{i\omega n(T/N)}, \quad (2.5)$$

where  $\phi$  is the velocity component of interest,  $T = 2\pi/\omega$  is the period, and  $k$  is an arbitrary integer.

Either the streamwise or the wall-normal component of velocity can be selected in order to measure the growth of T-S waves. In our simulations, the streamwise disturbance velocities are dominated by the boundary-layer streaks, which mask the T-S contribution in that direction. The wall-normal disturbance velocity of both the streaks and T-S waves remains of the same order of magnitude across the laminar region and is, therefore, a more suitable indicator of the strength of the T-S waves. In order to quantify the amplification of T-S waves, the wall-normal peak in the  $v$ -velocity spectra was obtained at every downstream location and compared between different simulations.

### 2.3. Resolution tests

The DNS code has been thoroughly validated by Zaki & Durbin (2005, 2006), who also provided guidelines on resolution requirements for transition studies. Additional resolution studies were carried out, where the nonlinear interaction of a T-S and a continuous mode is simulated upto and downstream of transition. Two continuous modes are considered: mode 2 and mode 5, as designated by their spanwise wavenumber.

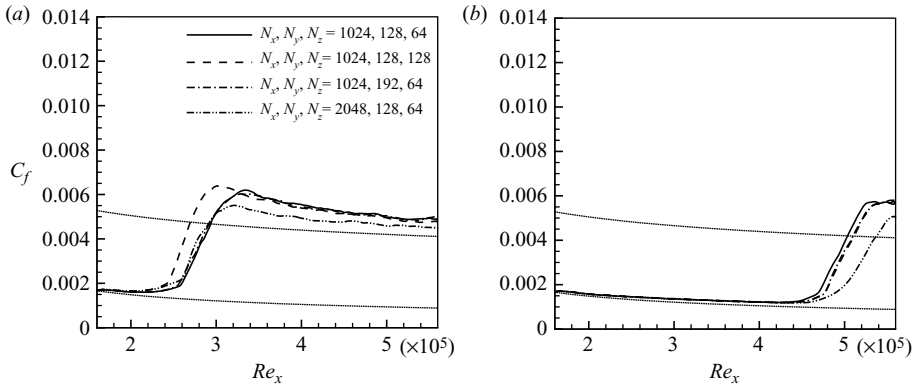


FIGURE 9. Grid resolution test: skin friction coefficient for transition due to the interaction of the T-S wave with the continuous modes (a) 2 and (b) 5.

We are mainly concerned with the early stages of the transition process. The inlet fundamental modes, their subharmonics and a few of the higher harmonics can all contribute to the nonlinear interactions preceding transition onset and, hence, must all be resolved. Breakdown to turbulence follows downstream. A full spectrum of perturbations emerges and the initial resolution becomes insufficient for capturing the turbulent boundary layer. An accurate representation of the fully turbulent region is not a goal here; resolving the fully turbulent region would greatly increase the grid node requirements, and as a result, limit the total number of interactions that can be simulated.

It is well known that skin friction is very sensitive to the spatial resolution (Jacobs & Durbin 2000). Figure 9 shows the skin friction curves for two sets of resolution tests. In each set, the base grid, which is composed of  $1024 \times 128 \times 64$  grid points in the streamwise, wall-normal and spanwise directions, is systematically refined along each axis. It is clear that the grid size does noticeably affect the transitional region where  $C_f$  rises from the laminar to the turbulent level and, as a result, the downstream Reynolds number where a fully turbulent solution is established. It is also worth noting that the effect of grid refinement is not the same in figures 9(a) and 9(b). In the former, finer grids lead to slightly accelerated transition whereas an opposite trend is observed in the latter. Our results also agree with Jacobs & Durbin (2000) who indicated that the skin friction curve can be brought close to the empirical turbulent value by increasing the streamwise resolution.

It is clear that the base grid resolution displayed in figure 9 under-resolves the turbulent region. The question, however, is how much does the under-resolution affect the quantities of interest here: the breakdown mechanism and transition location? We define the transition Reynolds number,  $Re_t$ , as the location where the slope of the  $C_f$  curve last changes signs, prior to its rise to the turbulent level. This value of  $Re_t$  marks the onset of the transition process seen in the simulations, namely the intermittent burst of turbulent patches which cause the rise in the skin friction curve and, once merged, constitute the fully turbulent boundary layer. The resulting  $Re_t$  is summarized in table 1. It is clear that  $Re_t$  is relatively insensitive to grid resolution.

Another question of concern is whether the base grid resolution faithfully reproduces the mechanics of transition. Although detailed plots are not shown for the various grid resolutions, all cases simulated in this work, at the various levels of

Case series	$N_x$	$N_y$	$N_z$	$Re_\tau$
Mode 2*	1024	128	64	214 000
Mode 2	2048	128	64	204 000
Mode 2	1024	192	64	205 000
Mode 2	1024	128	128	204 000
Mode 5*	1024	128	64	427 000
Mode 5	2048	128	64	437 000
Mode 5	1024	192	64	438 000
Mode 5	1024	128	128	436 000

TABLE 1. Transition Reynolds numbers for the resolution test of the mode 2 and mode 5 series; the asterisks label the standard resolution setting used in §§ 3 and 4.

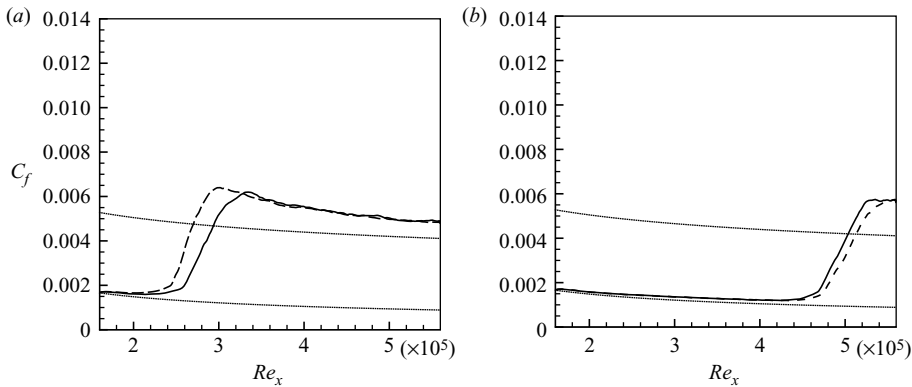


FIGURE 10. Skin friction coefficient for the spanwise domain size test of (a) mode 2 and (b) mode 5. Parameters are summarized in §§ 3 and 4. —,  $L_z = 8$ ; ---,  $L_z = 12$ .

grid resolution, breakdown to turbulence in the same manner, as will be discussed in § 3 and 4.

Since periodic boundary conditions are enforced in the spanwise direction, it is necessary to examine whether transition in our simulations is independent of the width of the computational domain. The outcome of doubling the spanwise extent of the domain, while maintaining the grid resolution in that direction unchanged, is shown in figure 10 and summarized in table 2. Again, transition onset is relatively insensitive to the domain size. It is also important to note that not only the transition Reynolds number, but also the transition mechanism is unaffected by doubling the spanwise extent of the domain. It will be shown in subsequent sections that breakdown in our simulations is preceded by the formation of  $\Lambda$ -structures. Both the streamwise and spanwise extents of these structures, and their relative arrangement remain unchanged when the domain size is doubled in the span. The independence of  $\Lambda$ -structures from the size of the computational domain was verified for all the simulations presented herein.

### 3. Mode locked interactions and breakdown to turbulence

This section describes the DNS of bi-modal interactions. A two-dimensional T-S wave and a continuous O-S mode were prescribed at the inlet of the computational domain and their evolution computed downstream. A large number of continuous

Case series	$L_z$	$Re_t$
Mode 2*	$8\delta_{99}$	214 000
Mode 2	$12\delta_{99}$	205 000
Mode 5*	$8\delta_{99}$	427 000
Mode 5	$16\delta_{99}$	436 000

TABLE 2. Transition Reynolds numbers for the dimension test of the mode 2 and mode 5 series; the asterisks label the standard resolution setting used in §§ 3 and 4.

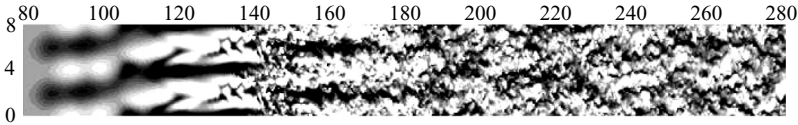


FIGURE 11. The contour of the streamwise fluctuation of the mode 2 case;  $t = 5\tau$ ;  $y = 0.5\delta_{99}$ . The spanwise coordinate is enlarged by a factor of 3. Contours are plotted in  $-0.2 < u < 0.2$ .

modes were investigated in Liu (2007), but only two,  $k_z = \{2k_z^0, 5k_z^0\}$ , will be discussed in this and the next section; they are representative of the two classes of outcomes from our simulations. Results from simulations of other continuous modes are included in the discussion, § 5. For each of the continuous modes considered, various amplitudes were prescribed at the inlet, and the influence on the amplification of the T-S wave and breakdown were evaluated.

Within the current theoretical framework, it is difficult to predict the outcome of the interaction between a continuous O-S and a discrete T-S mode. Each has a different phase speed, which excludes the possibility of nonlinear resonance. In addition, the mode shapes are concentrated at different heights within the boundary layer: the T-S mode has the majority of its energy in the near-wall region, whereas the continuous mode oscillates in the free stream and penetrates only the upper part of the boundary layer. As a result, the inner product of these two modes is small. Despite these caveats, DNS demonstrates that the interaction of a stable continuous mode with a T-S wave can provoke transition to turbulence. An interaction can be foreseen qualitatively: the continuous mode induces large-amplitude perturbation streaks within the boundary layer. Those streaks will cause three-dimensional distortions of the T-S. What this implies is studied by the following numerical simulations.

### 3.1. Modal interactions

Considered independently, the T-S and the continuous mode are innocuous. However, including both at the inflow plane, with amplitudes  $A_{TS}^0 = 1\%$ ,  $A_{con}^0 = 2.1\%$ , causes breakdown of the laminar boundary layer. A top view of the instantaneous perturbation contours is shown in figure 11. Instantaneous and time-averaged skin friction curves are shown in figure 12.

The  $C_f$  curve of this simulation is compared to the T-S control case in figure 12. As expected the oscillation of  $C_f$  is initially suppressed, but it then shoots up to the turbulent level. This bears on the seeming paradox reported by previous workers: a T-S wave is actually suppressed by jet-like perturbations, but transition is accelerated by free-stream turbulence. The swiftness of transition in this case makes the suppressive effect hard to discern in figure 12. The velocity spectra that are presented later in this section provide clearer evidence that the streaks reduce the amplification rate of T-S waves.

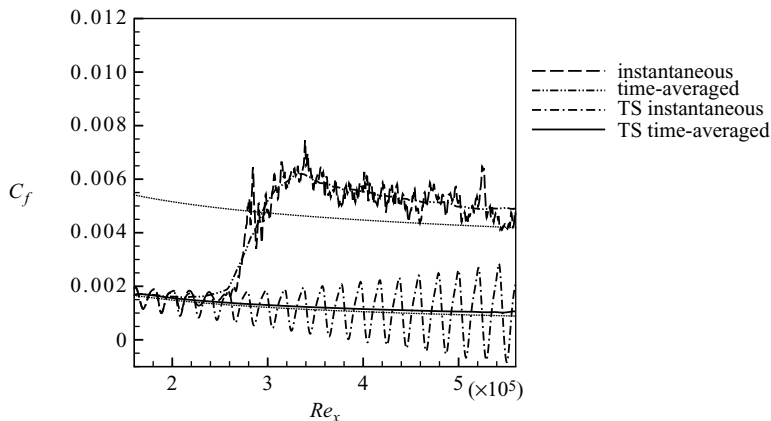


FIGURE 12. The skin friction coefficient *vs.* the  $Re_x$  of the mode 2 case. The lower curves show the T-S only case for reference;  $t = 3\tau$ .

### 3.1.1. The $\Lambda$ -structures

Breakdown of the boundary layer is preceded by the formation of  $\Lambda$ -shaped structures. It is not clear at this point, however, whether these  $\Lambda$ -structures have a similar origin to those emerging from the secondary instability of T-S waves (Herbert 1988). Such inference cannot be made from a single instant of the perturbation field. A series of snapshots is required to capture the evolution of these perturbations.

The lifetime of a pair of  $\Lambda$ -structures is shown by the time sequence in figures 13 and 14. Figure 13 is a top view of  $u'$  contours; figure 14 shows contours of  $v'$  and the in-plane velocity perturbation vectors, at the same time instances. The contour levels in the former figure are dominated by the large  $u$ -perturbation velocity of the boundary-layer streaks and the T-S waves are thus concealed. The T-S waves are visible in figure 14 only because the wall-normal perturbation remains comparable in magnitude for both the discrete mode and the boundary-layer streaks.

Figures 13(a) and 14(a) have mature  $\Lambda$ -structures positioned at  $x \sim 118$  and  $x \sim 126$ , respectively. The upstream event is of larger intensity. Attention should be focused, however, on the two modified three-dimensional T-S waves at  $x \sim 99$  and  $x \sim 108$ , respectively. These perturbations evolve into the  $\Lambda$ -structures farther downstream. In figures 13(b) and 14(b), as the pair of mature  $\Lambda$ -structures starts to break down, the valleys (dark regions) of the three-dimensional Tollmien–Schlichting waves move forward and begin to take on  $\Lambda$  shapes. It should be noted that the emerging structures are in a staggered position relative to the downstream pair. The emerging pair of  $\Lambda$ -structures intensifies in figures 13(c, d) and 14(c, d), and starts breaking down in figures 13(e) and 14(e). The lifetime of  $\Lambda$ -structures from inception to breakdown is approximately three T-S wavelengths. A fully turbulent state is established in the final time instant, figures 13(f) and 14(f). In the same snapshot, a new pair of  $\Lambda$ -structures can be seen emerging upstream, in a staggered arrangement.

The streamwise wavelength of the  $\Lambda$ -structures is nearly twice that of the discrete mode. This observation, and their staggered arrangement, suggest a connection to transition via the secondary instability of T-S waves. The connection is not, however, evident. The  $\Lambda$ -structures have a spanwise wavelength of  $4\delta_{99}$ , which is an order of magnitude smaller than predicted by a secondary instability of T-S waves alone (Herbert 1988). This spanwise size is, on the other hand, identical to the continuous

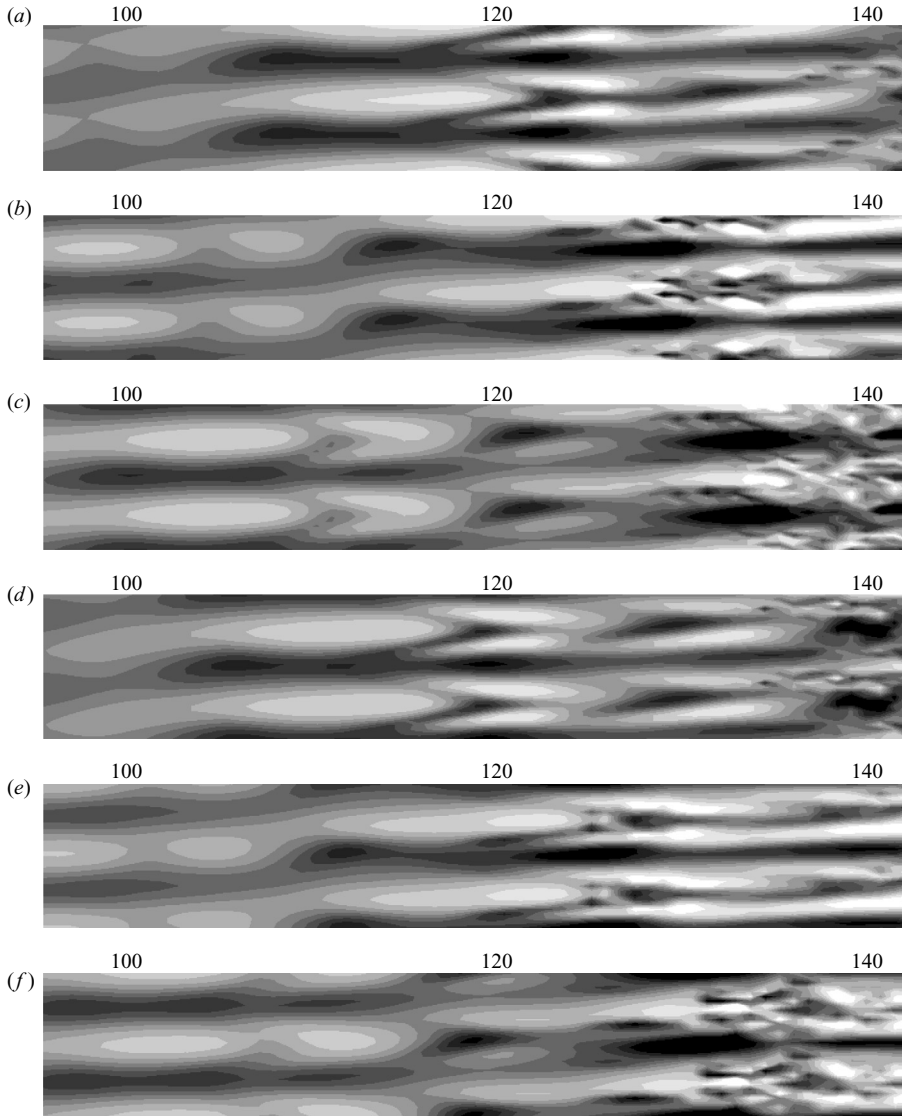


FIGURE 13. The instantaneous contour of the streamwise fluctuation of the mode 2 case in the  $(x, y)$ -plane;  $y = 0.5\delta_{99}$ . Contours are plotted in  $-0.2 < u < 0.2$ . Each frame is separated by  $\Delta t \sim 0.075\tau$ , where  $\tau$  is the flow-through time. The spanwise coordinate is not enlarged.

mode perturbation at the inflow. In other words, the spanwise wavenumber of the  $\Lambda$ -structures is locked to that of the continuous mode.

In secondary instability theory (Herbert 1988), the aligned and staggered arrangements of  $\Lambda$ -structures are an indication of fundamental and subharmonic resonances, respectively. As discussed above, the current  $\Lambda$ -structures appear in an alternating pattern: every two rows of  $\Lambda$ -structures are staggered relative to the following two rows, which are always at the centres of the streaks. The alternating arrangement is therefore a result of two effects: the locking of  $\Lambda$ -structures to the continuous mode and the unsteadiness of the continuous mode. This view is supported by our Floquet analysis, and other supporting evidence presented in § 5.

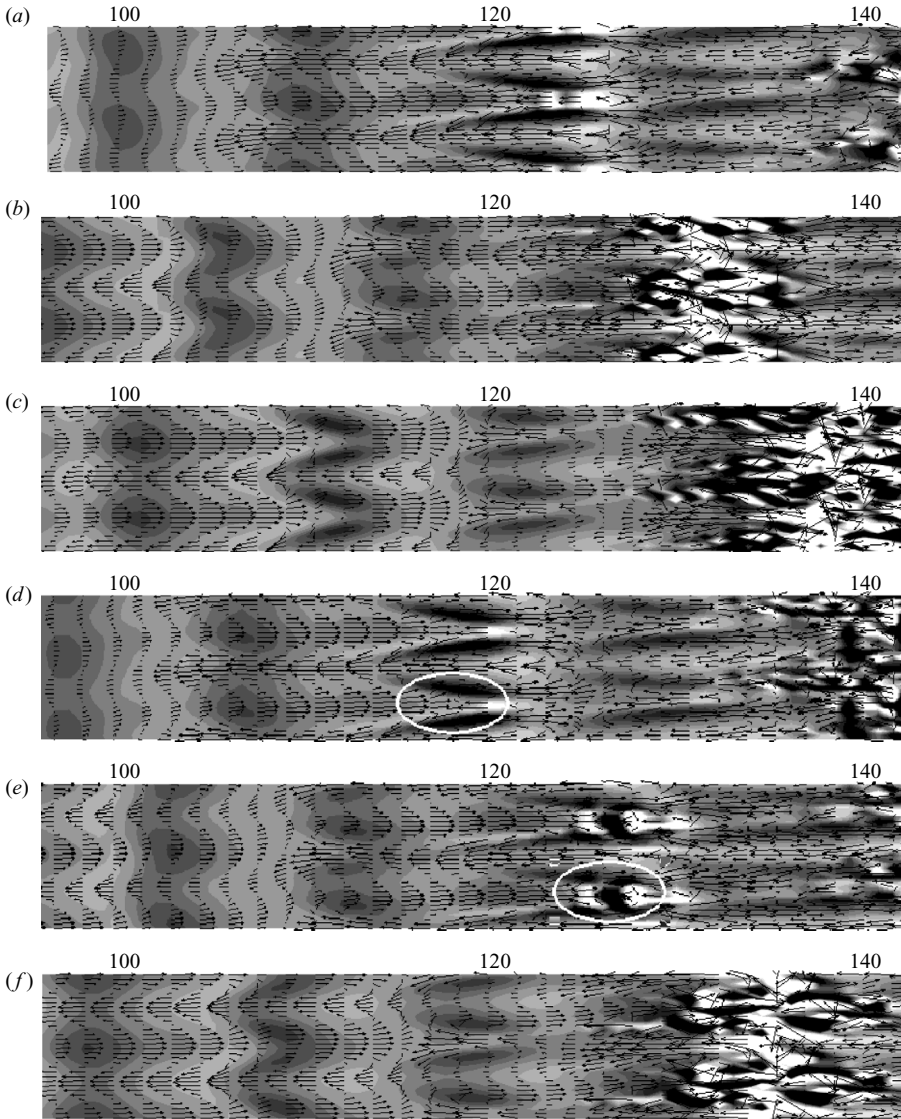


FIGURE 14. The instantaneous contour of the normal fluctuation and the vector plot of inplane components of the mode 2 case in the  $(x, y)$ -plane;  $y = 0.5\delta_{99}$ . Contours are plotted in  $-0.02 < v < 0.02$ . Each frame is separated by  $\Delta t \sim 0.075\tau$ , where  $\tau$  is the flow-through time. The spanwise coordinate is not enlarged.

The location where  $\Lambda$ -structures emerge oscillates in the streamwise direction. The streamwise undulation can be explained by the periodicity of the inlet modes. Though the final state of the boundary layer is turbulent and, hence, not periodic, the inlet modes are themselves periodic. Since the wavenumbers of the two modes are  $k_x^{TS} \sim 10k_x^{con}$ , in terms of wavelengths,  $10L^{TS} \sim L^{streak}$ . Note that the phase speeds of the two modes are  $c^{con} = 1$  and  $c^{TS} \sim 1/3$ . If each half-wavelength corresponds to a forward or to a backward jet, the time for a chosen T-S wave to reside in a specific jet is  $0.5L^{streak}/(c^{con} - c^{TS}) \sim 2.5L^{TS}/c^{TS}$ . Then within a period of modal interactions, about two  $\Lambda$ -structures would emerge within one negative jet (figure 14).

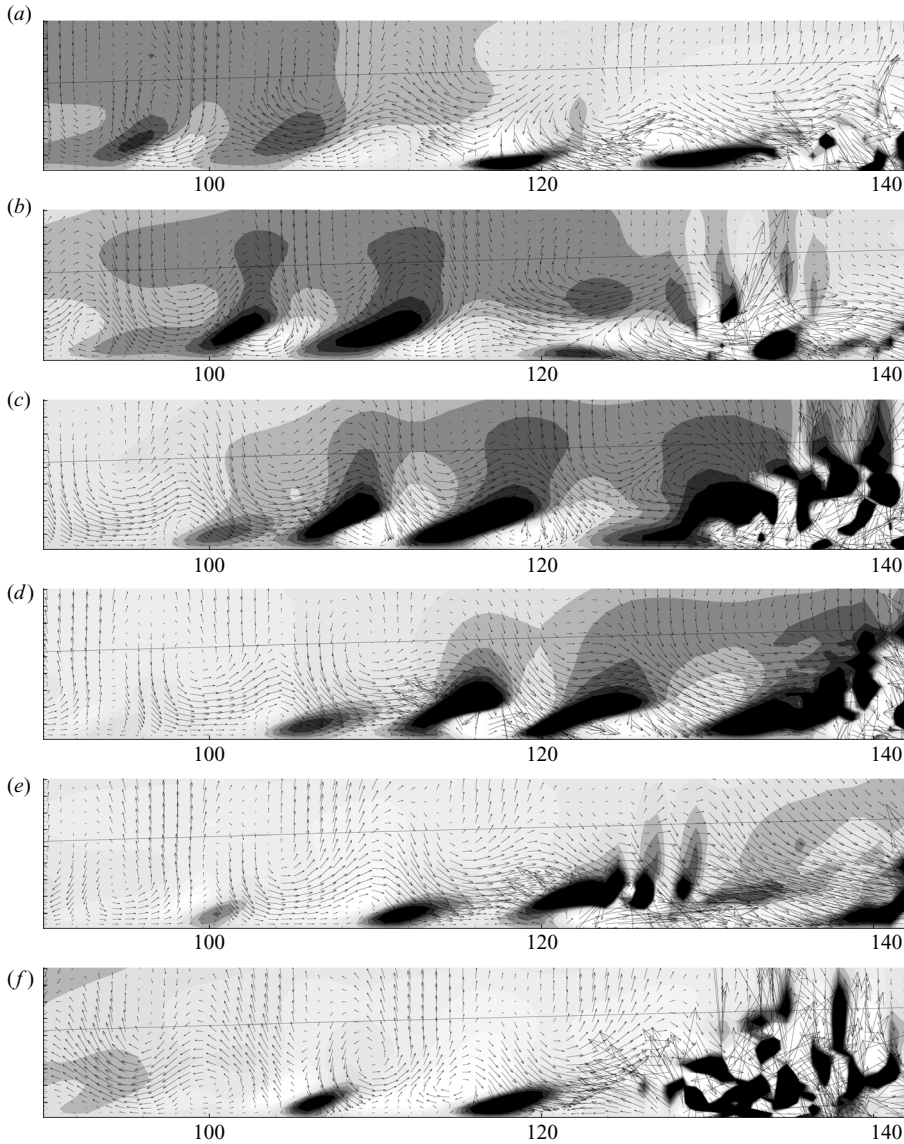


FIGURE 15. The instantaneous contour of the spanwise fluctuation and the vector plot of inplane components of the mode 2 case in the  $(x, y)$ -plane; the slice cuts through the centre of  $\Lambda$ -structures. Snapshots are taken corresponding to figures 13 and 14.

### 3.1.2. A side view of breakdown

Two-dimensional T-S waves are rolls of spanwise vortices while Klebanoff modes are forward and backward streamwise jets. Their interaction is best captured in figures 15 and 16 where side views of the velocity perturbations are plotted at the same time instants as shown in figures 13 and 14. The first sequence (figure 15) is a slice through the centre of  $\Lambda$ -structures while figure 16 cuts through a leg of a  $\Lambda$ -structure. The in-plane perturbations velocities are plotted as vectors, and the spanwise disturbance as background contours,  $-0.2\% < w < 2\%$ . In figure 15, the contours of  $w$ -perturbations are more intense because they lie at the centre of the

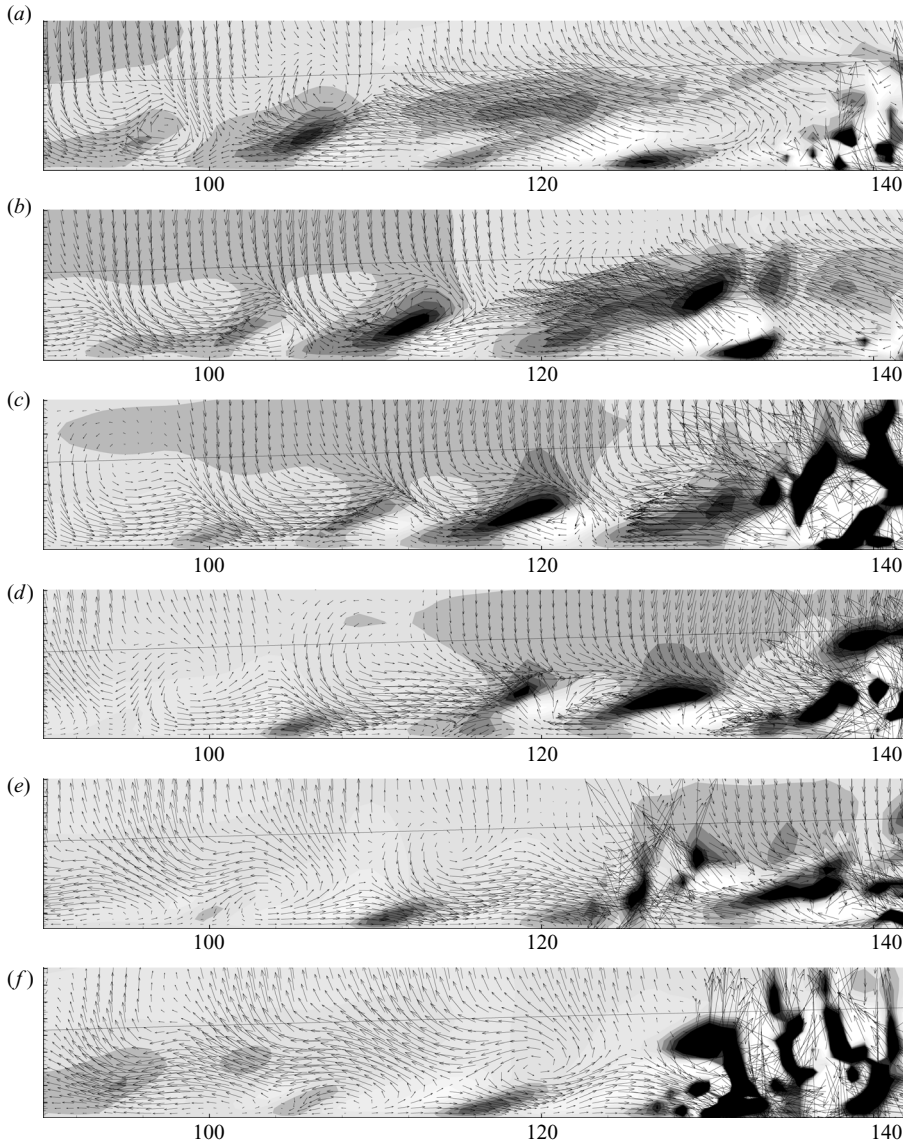


FIGURE 16. As figure 15 but the slice cuts through one leg of  $\Lambda$ -structures.

$\Lambda$ -structure, which straddles the forward and backward streaks (see figure 13). It is also in this plane that breakdown is initiated.

The breakdown mechanism captured in these figures is quite distinct from what Zaki & Durbin (2005, 2006) reported in simulations of continuous mode transition, and does not agree with descriptions of oblique T-S waves or streak instabilities. It appears as if the T-S disturbances act as a corrugated surface near the bottom of the boundary layer and move slowly downstream (figure 17, and also figure 26 discussed in the next section). The continuous mode disturbances generate boundary-layer streaks that lift up from the wall and sweep across the slow-moving sinusoidal T-S wave at the free-stream speed. Vortices are generated at the leading edge of the streaks. Because of the difference in phase speed of boundary-layer streaks and T-S waves,

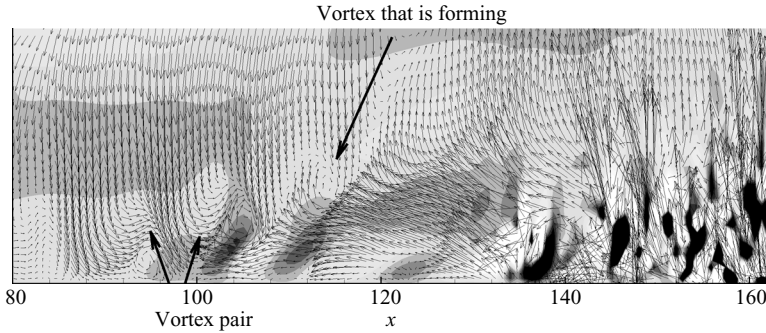


FIGURE 17. Illustration of the breakdown scenario for mode 2. An instantaneous contour of the spanwise fluctuation and with vectors of inplane components in an  $x$ - $y$  plane.

Case name	$A_{con}^0$ (%)	$A_{TS}^0$ (%)	$Re_t$
Mode 2	1.0	1.0	244 000
Mode 2	2.1	1.0	214 000
Mode 2	3.0	1.0	206 500

TABLE 3. The parameter setting and resulting  $Re_t$  data from the disturbance energy study of mode 2.

new vortices are continually shed. Vortices near the wall pair with the new vortices and convect them downward. It appears that the strong streamwise streaks (both forward and backward) hit the vortex pairs head-on and cause them to breakdown. This interaction of the streaks with the vortex pair is shown in side view, and also marked in the top view in figures 14(d, e). The marked regions of the figures show breakdown is initiated at the centre plane of the  $\Lambda$ -structures near the leading edge of the streaks.

### 3.2. The influence of modal amplitude

In order to investigate the effect of the streak amplitude,  $A_{con}^0$  was changed. Stronger ( $A_{con}^0 = 3\%$ ) and a weaker ( $A_{con}^0 = 1\%$ ) continuous modes were simulated. The numerical experiments reveal that all cases develop a clear lambda-vortex pattern. Table 3 summarizes the transition Reynolds number data, and figure 18 compares instantaneous skin friction curves from the various simulations. The results demonstrate that decreases in  $Re_t$  with increasing  $A_{con}^0$ . Despite the evidence in the literature that boundary layer streaks reduce the amplification rate of T-S waves, stronger streaks are observed to accelerate breakdown to turbulence in this, mode 2, series.

Two quantities are most likely to affect the transition in these simulations: (i) the local T-S wave amplitude and (ii) the strength of the boundary-layer streaks near the transition site. The oscillations of  $C_f$  on the left-hand side of figure 18 demonstrate that stronger streaks are more effective at suppressing the growth of T-S waves. Velocity spectra were computed using (2.5). The amplitude of the fundamental T-S frequency is shown in figure 19. The figure provides direct evidence that boundary-layer streaks impede the growth of T-S waves. So, we can conclude that in the mode 2 series, earlier transition is accomplished with reduced local T-S amplitude and stronger local Klebanoff streaks.

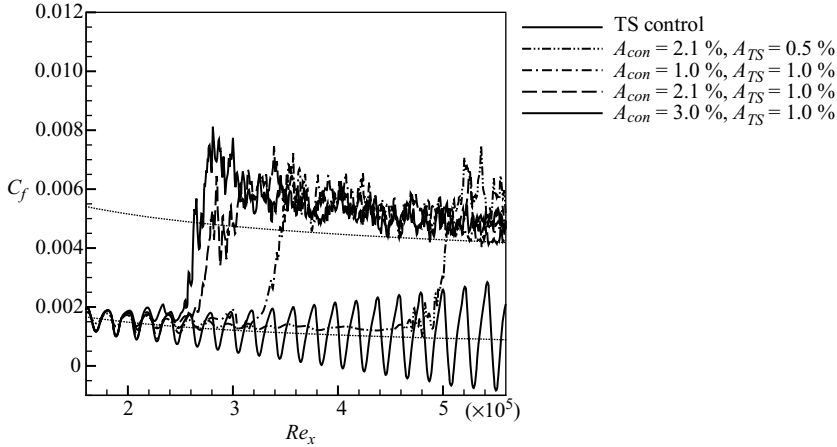


FIGURE 18. The skin friction of mode 2; effects of disturbance energy.

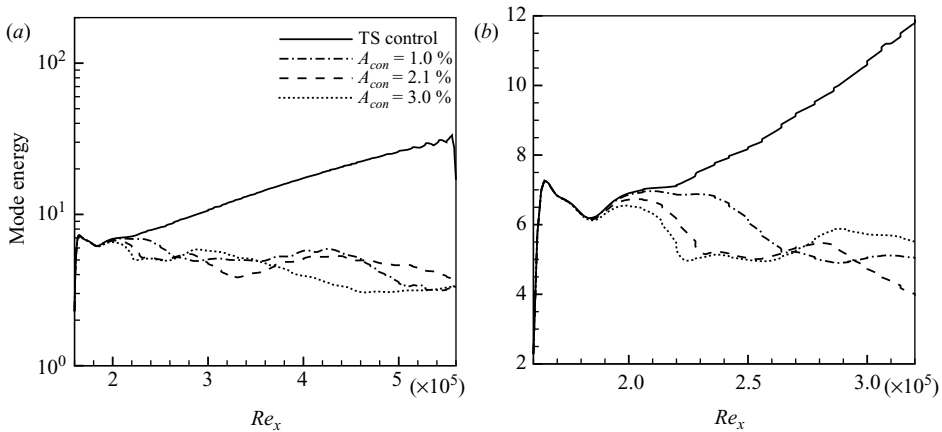


FIGURE 19. The amplitude of the fundamental T-S mode frequency for mode 2. A close up is shown in (b).

The suspicion that mode 2 breaks down through secondary instability of the T-S waves is further investigated by considering the perturbation spectra. Figure 20 shows the mode shape of the  $u$  and  $v$  velocity components at the subharmonic, fundamental, and first harmonic of the T-S mode frequency. The shape of the fundamental component agrees with figure 2 (it does not vanish on the top because the domain is cut to show the boundary layer clearly). Both the harmonic and subharmonic components have much of their energy inside the boundary layer, but are of smaller amplitude than the disturbance measured at the fundamental frequency.

Figure 21 shows the downstream evolution of the wall-normal maximum in the subharmonic and the first harmonic. The subharmonic shows clear dependence on the streak amplitude: stronger disturbances at the subharmonic of the T-S mode are observed in the presence of stronger streaks. More importantly, the subharmonic grows to a significant magnitude before the point of transition onset. The peak in the

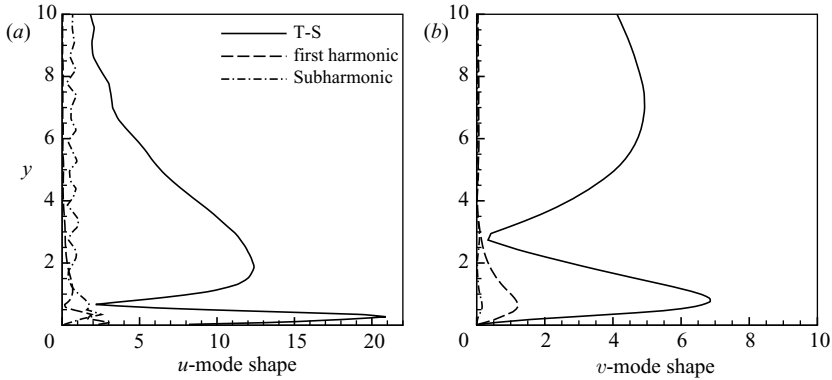


FIGURE 20. Profiles of (a) the streamwise and (b) wall-normal spectra.

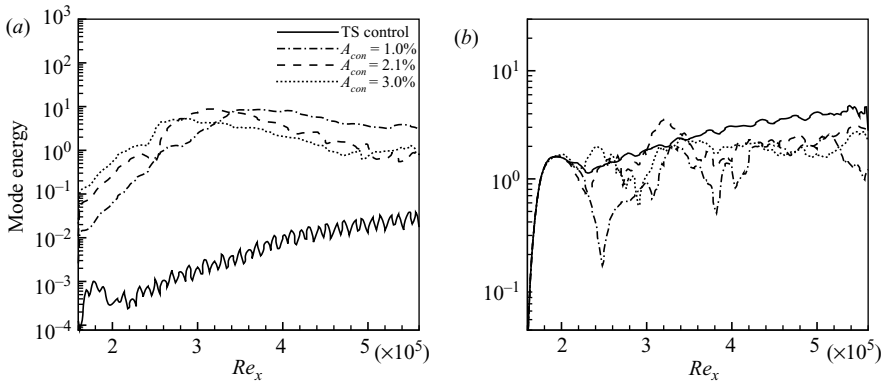


FIGURE 21. The amplitude of (a) the subharmonic and (b) first harmonic modes of the T-S perturbation.

amplification of the subharmonic component takes place near the breakdown location of the  $\Lambda$ -structures. On the contrary, the first harmonic shows little correlation with either the streak amplitude or the transition point. The spectra therefore supports the view that subharmonic instabilities of the T-S waves play a significant role in transition in the mode 2 series of simulations. This also is consistent with the staggered arrangement of the observed  $\Lambda$ -structures. However, a pure subharmonic would correspond to alternative rows of  $\Lambda$ -structures being staggered, rather than to pairs of rows forming into a staggered pattern.

#### 4. Detuned modal interactions and transition delay

The spanwise wavenumber of mode 5 follows the same naming convention as mode 2 and, therefore,  $k_z = 5k_z^0$ .

##### 4.1. Modal interactions

When both mode 5 and the T-S wave are included at the inflow, with amplitudes  $A_{con}^0 = 2.1\%$  and  $A_{TS}^0 = 1\%$ , the boundary layer undergoes transition to turbulence. An instant of the flow is shown in figure 22, a top view of the streamwise perturbation velocities inside the boundary layer. In this simulation,  $\Lambda$ -structures are also observed,

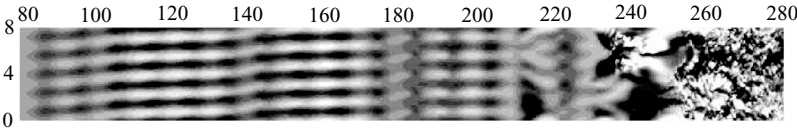


FIGURE 22. The contour of the streamwise fluctuation of the mode 5 case;  $t = 5\tau$ ;  $y = 0.5\delta_{99}$ . The spanwise coordinate is enlarged by a factor of 3. Contours are plotted in  $-0.2 < u < 0.2$ .

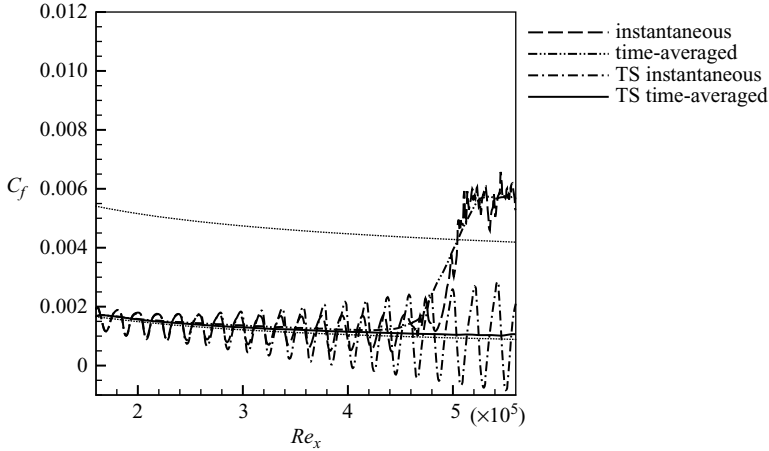


FIGURE 23. The skin friction coefficient *vs.* the  $Re_x$  of the mode 5 case with the T-S only case as control;  $t = 3\tau$ .

but are formed on negative  $u'$  streaks instead of the positive  $u'$  of the mode 2 simulations.

The skin friction curve is plotted in figure 23. By comparing it to the simulation of the T-S mode alone, the presence of boundary-layer streaks clearly suppresses the oscillation of  $C_f$  upstream of transition. Spectral amplitudes shown at the end of this section will confirm that the growth rate of T-S waves is reduced by the streaks. Moreover, the oscillations of  $C_f$  in the mode 5 case seem to be out of phase with those of the T-S control case. This indicates that the Klebanoff distortions modify the streamwise wave-length of the T-S waves. This small modification can be due to the mean flow distortion in the presence of nonlinear streaks. The large-amplitude streaks slightly alter the laminar boundary-layer profile and, as a result, the phase speed of the T-S waves. Since the inlet frequency of the perturbation is constant, the wavelength of the T-S modes is modified, although inappreciably.

#### 4.1.1. The $\Lambda$ -structures

After examining figures 24 and 25, it appears that the  $\Lambda$ -structures in the mode 5 case differ from those observed the mode 2 simulations. In mode 2, the spanwise wavelength of the  $\Lambda$ -structures is the streak width ( $\lambda_\Lambda = \lambda_{con}$ ), which is  $L_z/2 = 4\delta_{99}$ . In mode 5, the spanwise wavelength of the  $\Lambda$ -structures is nearly three times the width of the streaks ( $\lambda_\Lambda = 3\lambda_{con}$ ), which is approximately  $3/5 L_z = 4.8\delta_{99}$ . This observation indicates that the spanwise wavelength of the  $\Lambda$ -structures is not necessarily locked to the width of Klebanoff streaks. It is possible, nonetheless, that their span is an integer multiple of the streak width. The DNS results alone do not provide sufficient evidence

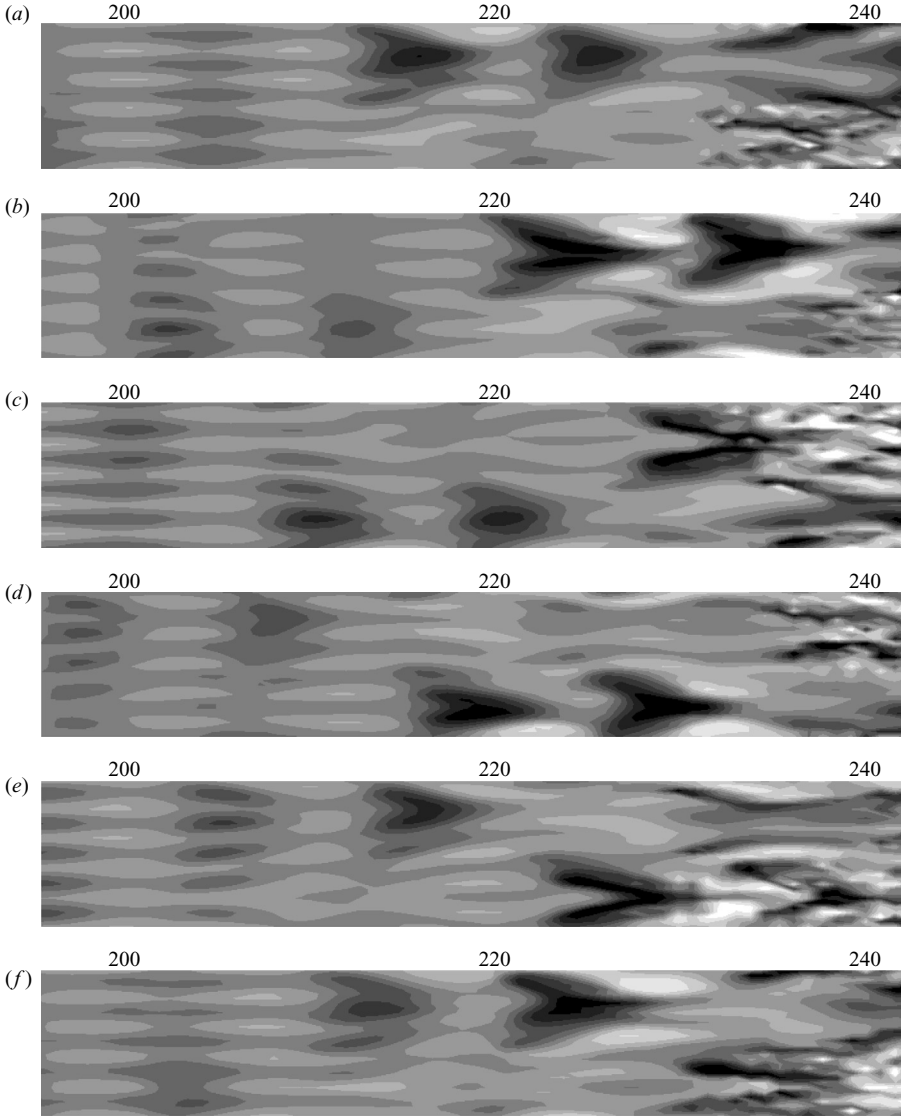


FIGURE 24. The instantaneous contour of the streamwise fluctuation of the mode 5 case in the  $(x, y)$ -plane;  $y = 0.5\delta_{99}$ . Contours are plotted in  $-0.2 < u < 0.2$ . Each frame is separated by  $\Delta t \sim 0.1\tau$ , where  $\tau$  is the flow-through time. The spanwise coordinate is not enlarged.

to support this assertion. The Floquet analysis described in § 5.1, on the other hand, provides the theoretical basis predicting the spanwise extent of the  $\Lambda$ -structures.

In the mode 5 case, the  $\Lambda$ -structures still appear in an alternating pattern: two aligned  $\Lambda$ -structures followed by another two aligned  $\Lambda$ -structures but in staggered position. However, only one  $\Lambda$  can be found in a row because only one fits into the computation domain ( $\lambda_{\Lambda} = 0.6L_z$ ). An oscillation of the starting location of the  $\Lambda$ -structures is also present in this case.

The appearance of the  $\Lambda$ -structures in figures 24 and 25 is quite different from their mode 2 counterpart. Recall the  $\Lambda$ -structures in mode 2 are just a  $\Lambda$ -shaped concentration of negative  $v'$  centred on a forward jet. In the case of mode 5, on

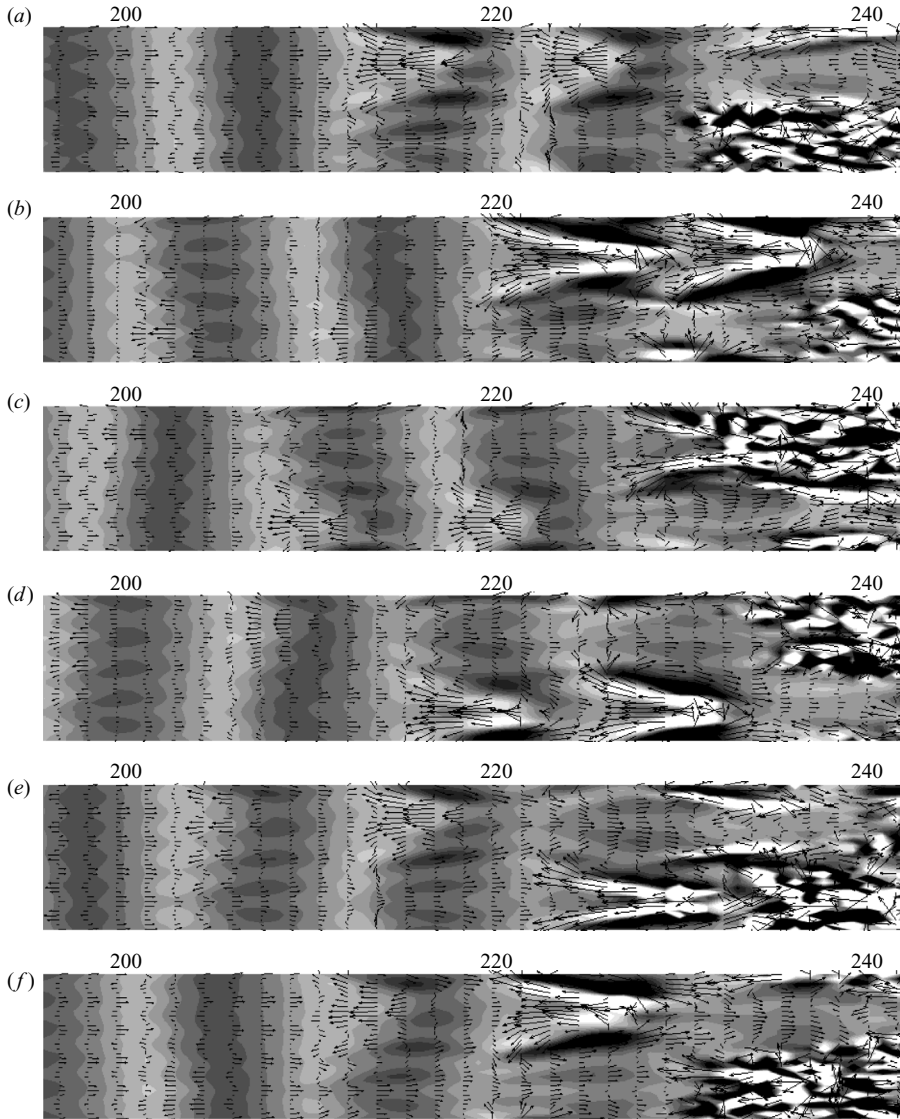


FIGURE 25. The instantaneous contour of the normal fluctuation and the vector plot of inplane components of the mode 5 case in the  $(x, y)$ -plane;  $y = 0.5\delta_{99}$ . Contours are plotted in  $-0.02 < v < 0.02$ . Each frame is separated by  $\Delta t \sim 0.1\tau$ , where  $\tau$  is the flow-through time. The spanwise coordinate is not enlarged. The vector length is plotted as grid units magnitude = 10.

the other hand, the  $\Lambda$ -structures have a strong backward jet at their centre, with a spanwise size identical to the width of the structure itself rather than the width of the Klebanoff streaks. The core of the  $\Lambda$ -structures is a  $\Lambda$ -shaped concentration of positive  $v'$ , which is flanked by negative  $v'$ . These differences suggest the  $\Lambda$ -structures from the two series of simulations might be generated by different mechanisms.

#### 4.1.2. A side view of breakdown

In the mode 2 simulations, the relative phase speed of the boundary-layer streaks and the T-S waves caused vortical shedding. The strong streamwise perturbation

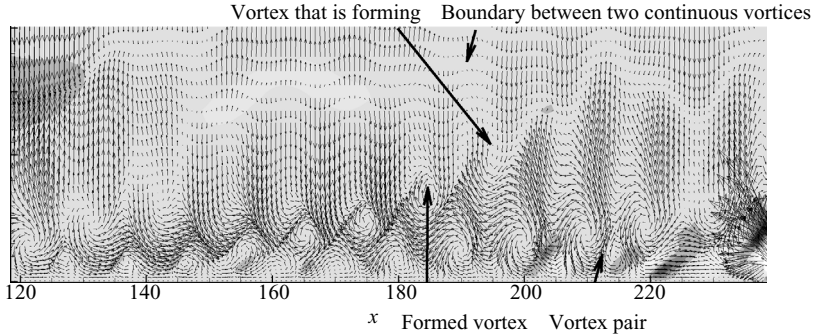


FIGURE 26. Mode 5. An instantaneous contour of the spanwise fluctuation with vectors of the inplane components in an  $(x, y)$ -plane. The vector length is plotted as grid units/magnitude = 20.

streaks, or jets, seemingly impacted the induced vortex pairs head-on, thus causing their breakdown. In the mode 5 simulations, however, the boundary-layer streaks generated owing to the continuous mode are much weaker. Instead, the vortex pairs are destabilized through an interaction with subsequently shed and amplifying vortices (figure 26). The time sequence of the interaction leading to breakdown is shown in figures 27 and 28. The former figure shows the perturbation field in a plane which bisects the  $\Lambda$ -structure, and latter is a cut through one leg of the  $\Lambda$  shape.

While  $\Lambda$ -structures precede transition in both mode 2 and 5 simulations, the details of their makeup and breakdown differ. Perhaps the two sets of simulations represent different types of the same breakdown mechanism, similar for example to K- and H-types of secondary instabilities.

#### 4.2. The influence of modal amplitude

The influence of the initial amplitudes  $A_{TS}^0$  and  $A_{con}^0$  are also investigated for mode 5. Similar to the numerical experiments for mode 2, stronger and weaker O-S continuous modes,  $A_{con}^0 = 3\%$  and  $A_{con}^0 = 1\%$  respectively, were simulated.

Table 4 summarizes the transition-Reynolds-numbers data and figure 29 compares the instantaneous skin friction from the various simulations. Once again, the weaker T-S waves delay transition. The effect of the inlet amplitude of the continuous mode,  $A_{con}^0$ , is opposite to the trend recorded in the mode 2 simulations. In the latter case,  $Re_t$  decreased with increasing  $A_{con}^0$ : stronger streaks promote transition in that series. In the current case of mode 5,  $Re_t$  increases with an increasing  $A_{con}^0$  or, equivalently, transition is promoted by decreasing the streak amplitude. It should be noted, however, that in the absence of streaks, the limit  $A_{con}^0 = 0$ , transition does not take place. Hence,  $Re_t$  must decrease, then increase — meaning there is an optimal  $A_{con}^0$  for mode 5.

Both figure 29 and the spectral amplitude, figure 30, confirm that stronger streaks are more effective at suppressing the growth of T-S waves. As a result, in the mode 5 series, early transition is associated with lower Klebanoff streak magnitude and higher T-S amplification rates.

In all the transitional cases from mode 5 series, breakdown was preceded by the formation of  $\Lambda$ -structures. The transition location for  $\{A_{TS}^0 = 1.0\%, A_{con}^0 = 3.0\%\}$  is close to the exit plane of the computational domain. It is difficult to infer whether these two cases reach the breakdown stage based solely on their skin friction curves.

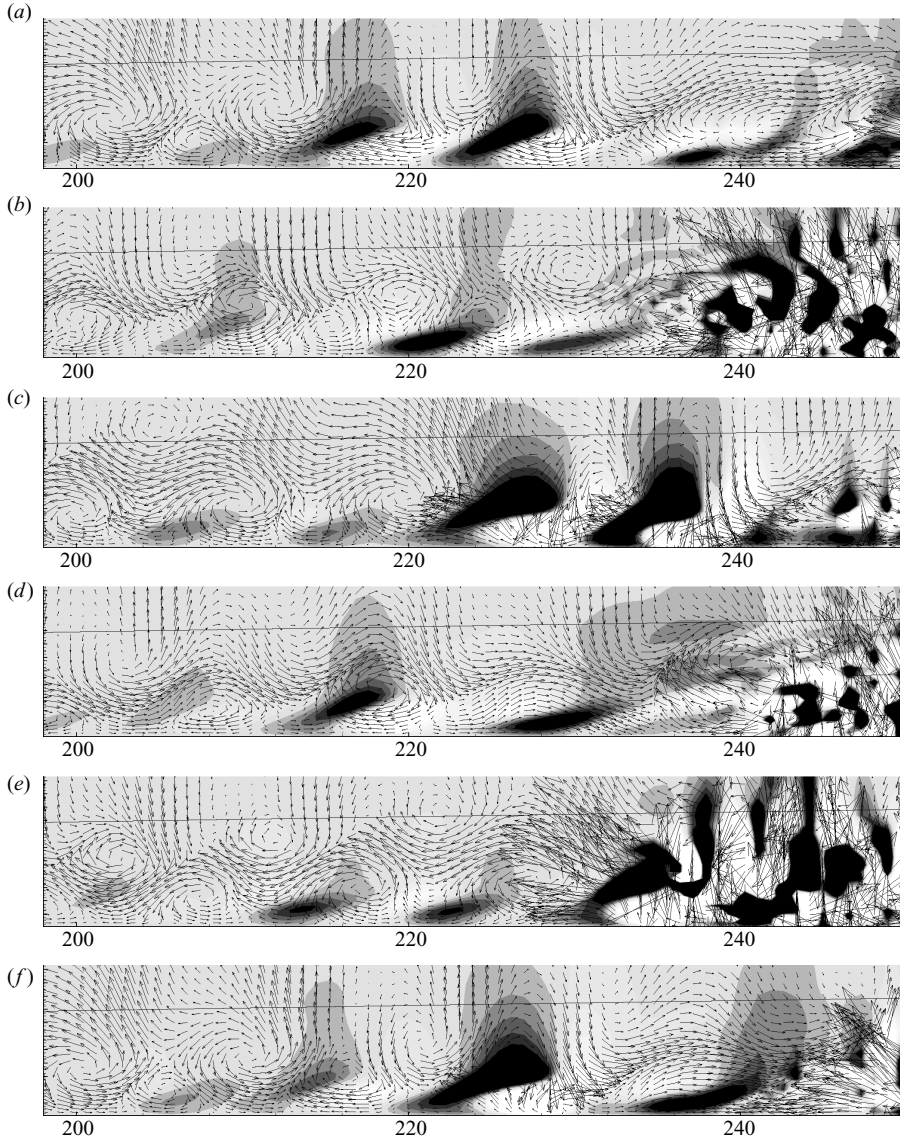


FIGURE 27. The instantaneous contour of the spanwise fluctuation and the vector plot of inplane components of the mode 5 case in the  $(x, y)$ -plane; the slice cuts through the centre of  $\Lambda$ -structures. The vector length is plotted as grid units/magnitude = 20. Snapshots are taken corresponding to figures 24 and 25.

The velocity contours in figure 31, however, show the formation of distinct  $\Lambda$ -structures near the outlet in the former case.

The spectral amplitudes at the fundamental, harmonic and subharmonic frequencies were computed for mode 5. Figure 32 shows the sub- and first harmonic components. The subharmonic again shows a clear dependence on the streak amplitude; stronger streaks introduce stronger subharmonic disturbances. The transition locations are less clear in figure 32(a) than those in the mode 2 counterpart (figure 20a). Nonetheless, a correlation between the development of subharmonic disturbance and transition

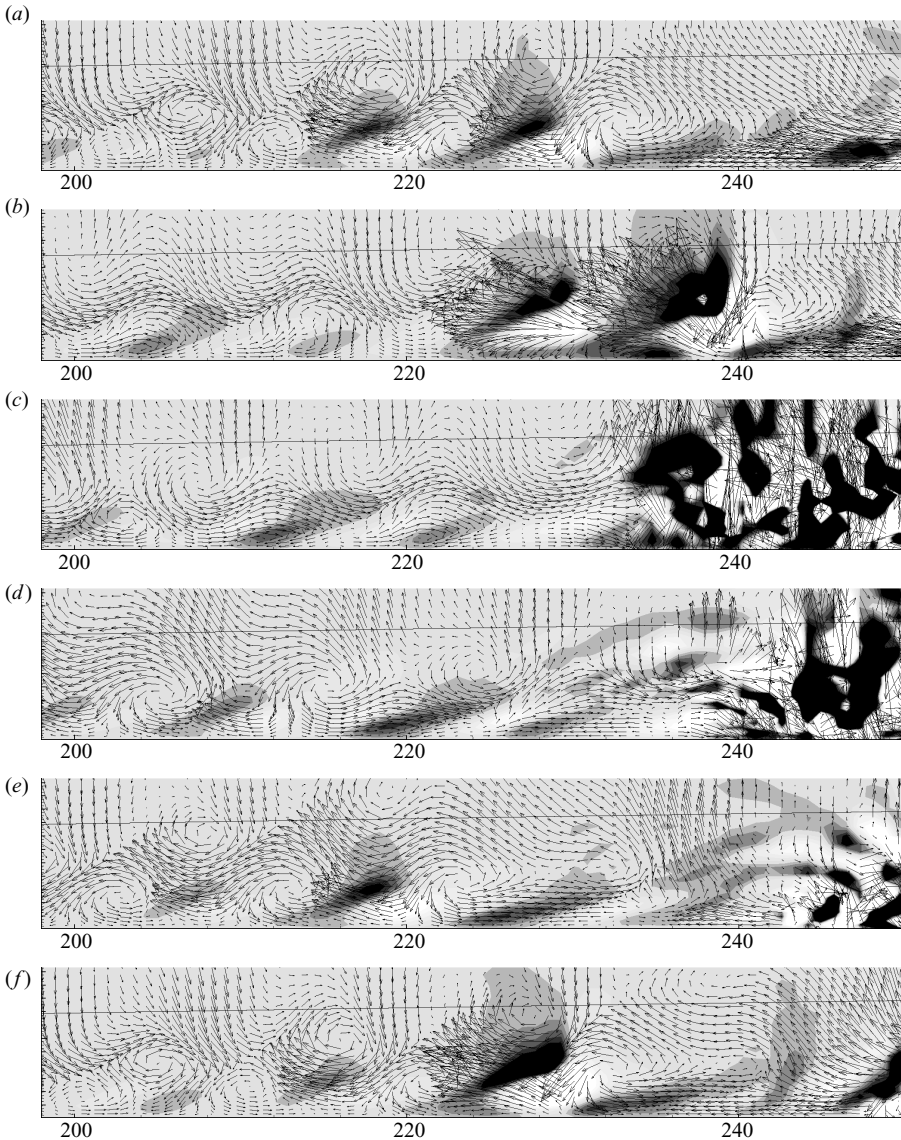


FIGURE 28. As figure 27 but the slice cuts through one leg of  $\Lambda$ -structures.

exists. The first harmonic shows similar trends to the fundamental mode whose growth rate is reduced by the presence of boundary-layer streaks.

Figures 33 shows the streamwise and wall-normal spectral components at the fundamental, harmonic and subharmonic frequencies. Again, the shape of the amplitude at the fundamental frequency agrees with figure 2. The other components have much of their energy well inside the boundary layer.

## 5. Discussion

At the interface of orderly and bypass transition lies a regime where T-S waves and boundary-layer streaks are both present within the flow and can interact. The interaction was investigated using direct numerical simulations. Independently, the

Case name	$A_{con}^0$ (%)	$A_{TS}^0$ (%)	$Re_t$
Mode 5	1.0	1.0	400 000
Mode 5	2.1	1.0	427 000
Mode 5	3.0	1.0	509 000

TABLE 4. The parameter setting and resulting  $Re_t$  data from the disturbance energy study of mode 5.

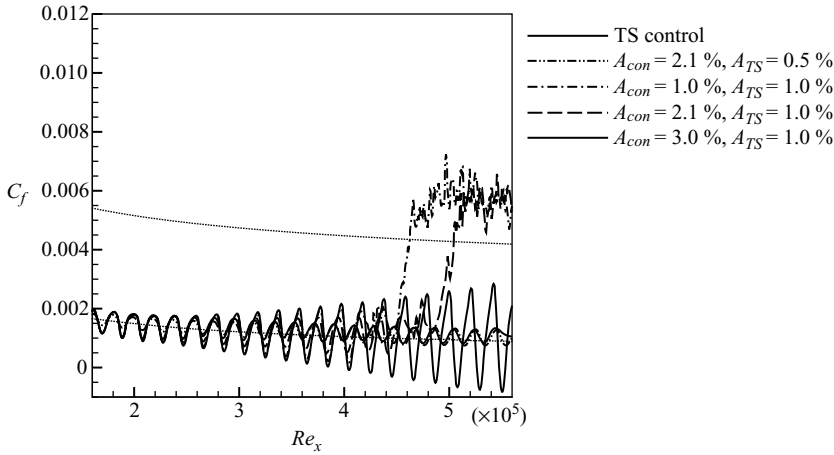


FIGURE 29. The skin friction of mode 5; effects of disturbance energy.

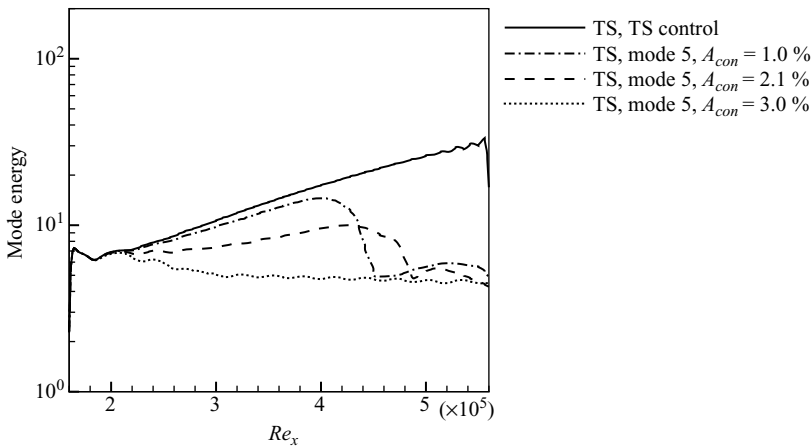


FIGURE 30. The amplitude of the fundamental T-S mode, mode 5.

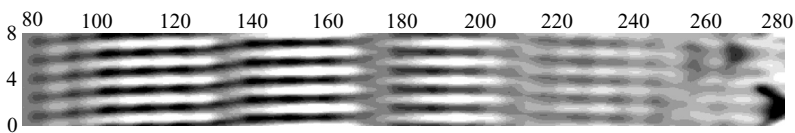


FIGURE 31. The contour of the streamwise fluctuation of the mode 5 case;  $A_{TS}^0 = 1.0\%$ ,  $A_{con}^0 = 3.0\%$ ;  $t = 3\tau$ ;  $y = 0.5\delta_{99}$ .

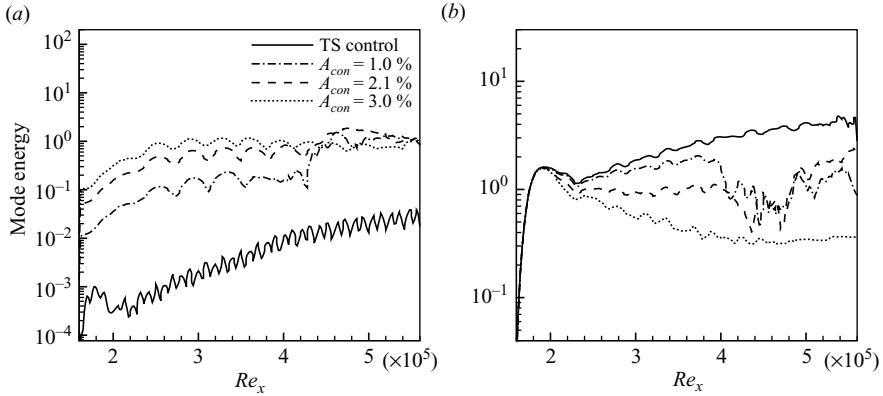


FIGURE 32. The amplitude of (a) the subharmonic and (b) first harmonic modes of the T-S perturbation.

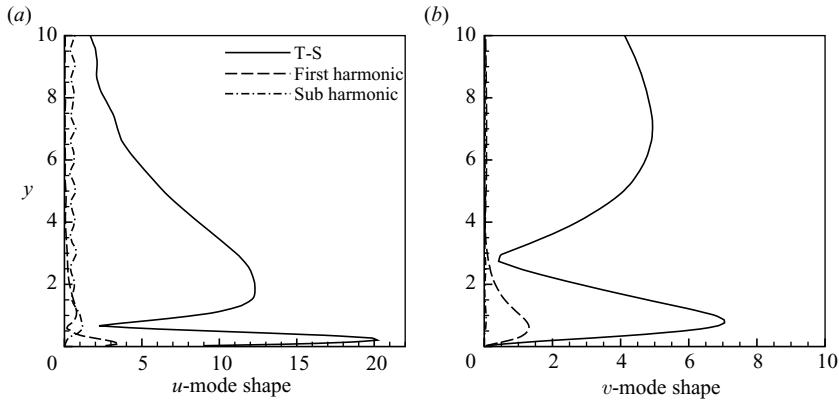


FIGURE 33. Profiles of (a) the streamwise and (b) wall-normal spectra.

discrete and the continuous modes in our simulations do not breakdown within the computational domain. However, the flow becomes transitional when both modes are present. The influence of the streaks on the growth rate of T-S modes is consistent: stronger streaks suppress the amplification of T-S waves. On the other hand, the size of the  $\Lambda$ -structures which precede breakdown and the location of transition onset have a more complex dependence on the streak amplitude and spanwise wavenumber.

### 5.1. The Floquet analysis

Floquet analysis provides some understanding of the DNS results. The analysis involves solving the stability problem for the Navier–Stokes equations, linearized about a base flow which is a superposition of the Blasius profile, a saturated T-S wave, and Klebanoff streaks. The base flow is therefore,

$$U(y, z, t) = U_0(y)\mathbf{e}_x + A(u_{TS}(x, y, t)\mathbf{e}_x + v_{TS}(x, y, t)\mathbf{e}_y) + Bu_K(y, z)\mathbf{e}_x, \quad (5.1)$$

where  $u_{TS}$  and  $u_K$  are periodic functions of the form  $u_{TS}(k_x x)$  and  $u_K(k_z z)$ ;  $k_x$  and  $k_z$  are wavenumbers of the T-S and Klebanoff distortions, respectively.

The disturbance equations are given below in terms of the disturbance velocity,  $u_3, v_3, w_3$ , and vorticity,  $\xi_3, \eta_3, \zeta_3$ , components.

$$\begin{aligned} & \frac{1}{Re} \nabla^2 \eta_3 - (U_0 - c) \frac{\partial \eta_3}{\partial x'} - U_0' \frac{\partial v_3}{\partial z} - A \left[ u_{TS} \frac{\partial \eta_3}{\partial x'} + v_{TS} \frac{\partial \eta_3}{\partial y} \right. \\ & \quad \left. + \frac{\partial u_{TS}}{\partial x'} \eta_3 - \frac{\partial v_{TS}}{\partial x'} \xi_3 + \left( \frac{\partial u_{TS}}{\partial y} - \frac{\partial v_{TS}}{\partial x'} \right) \frac{\partial v_3}{\partial z} \right] \\ & - B \left[ u_K \frac{\partial \eta_3}{\partial x'} + \frac{\partial^2 u_K}{\partial y \partial z} v_3 + \frac{\partial^2 u_K}{\partial z^2} w_3 + \frac{\partial u_K}{\partial y} \frac{\partial v_3}{\partial z} - \frac{\partial u_K}{\partial z} \frac{\partial v_3}{\partial y} \right] = \frac{\partial \eta_3}{\partial t}, \quad (5.2) \end{aligned}$$

$$\begin{aligned} & \frac{1}{Re} \nabla^2 (\nabla^2 v_3) - (U_0 - c) \frac{\partial \nabla^2 v_3}{\partial x'} + U_0'' \frac{\partial v_3}{\partial x'} \\ & - A \left[ u_{TS} \frac{\partial \nabla^2 v_3}{\partial x'} + v_{TS} \frac{\partial \nabla^2 v_3}{\partial y} + \frac{\partial v_{TS}}{\partial x'} \left( \frac{\partial \zeta_3}{\partial y} + \frac{\partial \eta_3}{\partial z} \right) + \frac{\partial u_{TS}}{\partial x'} \left( \frac{\partial \zeta_3}{\partial x'} + \frac{\partial \xi_3}{\partial z} \right) \right. \\ & \quad \left. + \frac{\partial \zeta_{TS}}{\partial x'} \left( 2 \frac{\partial u_3}{\partial x'} + \frac{\partial v_3}{\partial y} \right) + \frac{\partial \zeta_{TS}}{\partial y} \frac{\partial v_3}{\partial x'} + \frac{\partial^2 \zeta_{TS}}{\partial x'^2} u_3 + \frac{\partial^2 \zeta_{TS}}{\partial x' \partial y} v_3 \right] \\ & - B \left[ u_K \frac{\partial \nabla^2 v_3}{\partial x'} - \left( \frac{\partial^2 u_K}{\partial y^2} - \frac{\partial^2 u_K}{\partial z^2} \right) \frac{\partial v_3}{\partial x'} - 2 \frac{\partial u_K}{\partial z} \frac{\partial \xi_3}{\partial x'} - 2 \frac{\partial^2 u_K}{\partial y \partial z} \frac{\partial w_3}{\partial x'} \right] = \frac{\partial \nabla^2 v_3}{\partial t}, \quad (5.3) \end{aligned}$$

$$\frac{\partial u_3}{\partial x'} + \frac{\partial v_3}{\partial y} + \frac{\partial w_3}{\partial z} = 0. \quad (5.4)$$

The Floquet expansion for the secondary disturbance takes the form,

$$v_3 = e^{\sigma t} e^{i\gamma x'} e^{i\beta z} \sum_{n=-\infty}^{\infty} \sum_{m=-\infty}^{\infty} \hat{v}_{n,m}(y) e^{i(nk_x x' + mk_z z)}, \quad (5.5)$$

where  $x' = x - ct$  is the streamwise position in the frame of the T-S wave. Here we consider the temporal stability problem, where the real part of  $\sigma$  is the growth rate. The wavenumbers  $\gamma$  and  $\beta$  are those of the disturbance. Periodicity in two directions greatly complicates the analysis; details can be found in Liu (2007).

The above system recovers the equations of Herbert (1988) when the streak amplitude,  $B$ , vanishes and the base flow is periodic in one direction only. The eigensolutions in this limit are the secondary instability modes of two-dimensional T-S waves. When  $A$  is set to zero, the system reduces to the stability equations of the Blasius profile in the presence of steady streaks only. These equations were used by Cossu & Brandt (2004) to demonstrate the stabilizing effect of streaks on the growth rate of primary T-S waves. Our algorithm for solving the secondary stability problem for a double-periodic base flow was validated in the above two limits. In the absence of streaks, the secondary instability of T-S waves matches that in Herbert (1988). When the streaks act alone,  $A = 0$ , the Floquet analysis predicts a stabilizing effect; the primary T-S waves have a lower amplification rate owing to the influence of the streaks, consistent with Cossu & Brandt (2004).

Both the primary T-S waves and Klebanoff streaks are retained to investigate the influence of streak amplitude on secondary instability. The results for mode 2 are shown in figure 34. When the streaks reach an intensity of approximately 15 %, they

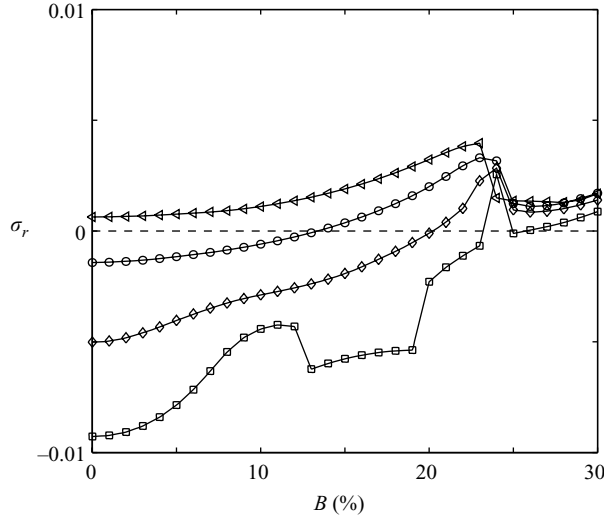


FIGURE 34. Effect of the streak strength  $B$  of mode 2 on the growth rate  $\sigma_r$ . The subharmonic instability in  $x$  ( $NA = 1$ ) and fundamental in  $z$  ( $NB = 2$ ) is considered at different amplitudes of the T-S waves:  $\square$ ,  $A = 0.2\%$ ;  $\diamond$ ,  $A = 0.5\%$ ;  $\circ$ ,  $A = 1.0\%$ ;  $\triangleleft$ ,  $A = 1.5\%$ .

destabilize T-S waves of 1% amplitude. The  $A = 1.5\%$  wave, which is subject to secondary instability for all values of  $B$ , shows a significant increase in growth rate when  $B \approx 20\%$ . Streak amplitudes of 15–20% are in line with those seen in DNS. Figure 34 corresponds to Floquet modes that are subharmonic in  $x$  and fundamental in  $z$  ( $\epsilon_z = 0$  in equation (5.6)). Hence, the formation of  $\Lambda$ -structures can be attributed to a secondary instability that locks onto the Klebanoff streak width.

The limit  $B \rightarrow 0$  corresponds to the results of Herbert (1988). The optimal growth for Herbert’s case occurs at a spanwise wavelength of around ten boundary-layer thicknesses. That is almost an order of magnitude wider than the  $\Lambda$ -structures seen in the present DNS. However, in Herbert’s analysis it is supposed that the boundary layer is subjected to arbitrary disturbances, from which the optimally growing perturbation is extracted. In the present case, free-stream disturbances induce strong Klebanoff streaks near the wall and those set the wavelength that distorts the T-S waves. Natural Klebanoff streaks have a wavelength of about one boundary-layer thickness. The present ansatz explains how an instability can lock onto that length scale.

As we have seen, mode 5 behaves differently from mode 2. In Floquet analysis, a detuning factor is defined as

$$\epsilon_z = \inf_{-\infty < m < \infty} \min \left( 2 \left| \frac{\beta}{k_z} - m \right|, 1 \right), \tag{5.6}$$

where  $k_z$  is the streak wavenumber. For mode 2,  $k_z = 2k_{z0} = 2 \times 2\pi/L_z$ , and for mode 5,  $k_z = 5k_{z0}$ . The fundamental disturbance mode is represented by (5.5) with  $\beta = k_z$  so that  $\epsilon_z = 0$ ; the subharmonic case is  $\beta = k_z/2$  so  $\epsilon_z = 1$ . For mode 5, each  $\epsilon_z$  corresponds to wavenumbers

$$k_z = \frac{1}{2}\epsilon_z 5k_{z0}, \left(1 - \frac{1}{2}\epsilon_z\right) 5k_{z0}, \left(1 + \frac{1}{2}\epsilon_z\right) 5k_{z0} \dots \tag{5.7}$$

in the series of (5.5), where  $k_{z0} = 2\pi/L_z$  (equation (2.4)).

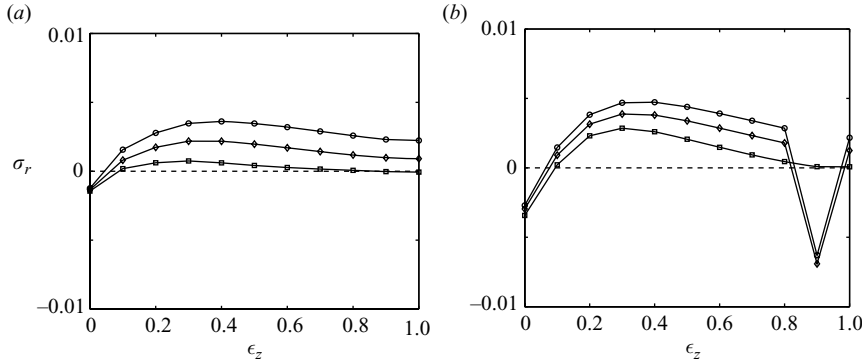


FIGURE 35. Effect of the spanwise detuning factor  $\epsilon_z$  on the growth rate of the (a) fundamental and (b) the subharmonic (in  $x$ ) instability of mode 5. The streak amplitude,  $B = 10\%$ . Three T-S wave amplitudes are shown:  $\square$ ,  $A = 1.5\%$ ;  $\diamond$ ,  $A = 2.0\%$ ;  $\circ$ ,  $A = 2.5\%$ .

Mode 5 has maximum growth for a detuning factor between 0 and 1. That explains why the width of the  $\Lambda$ -structures does not lock onto the Klebanoff wavelength, even though that is the source of spanwise forcing. Figure 35 shows the dependence of the maximum growth rate of the secondary instability on the detuning factor. Maximum amplification is around  $\epsilon_z = 0.4$ , but the unstable response is broad.  $\epsilon_z = 0$  is always stable. Hence, the perturbation induced by mode 5 does not directly stimulate an instability. This provides an understanding of the different responses that we have seen for modes 2 and 5.

Based on both the Floquet analysis and the DNS, the streaks play a dual role in the breakdown mechanism under investigation. First, they reduce the growth rate of the primary T-S waves; this observation is consistent with the previous work (Cossu & Brandt 2004; Fasel 2002) for steady streaks. In the meantime, the streaks can promote the secondary instability of the primary T-S modes. The secondary eigenmodes can be either locked to the streak spanwise wavenumber or detuned, as exemplified by the mode 2 and mode 5 cases, respectively.

### 5.2. Further simulations and concluding remarks

Further simulations were carried out in order to investigate the influence of (a) the spanwise wavenumber and (b) the unsteadiness of the streaks on transition. A range of spanwise wavenumbers of the inlet continuous mode were considered, and two amplitudes were specified,  $A_{con} = \{2.1\%, 1.0\%\}$ . The instantaneous skin friction curves from these simulations are shown in figure 36. A complete account of the combined effect of disturbance energy and spanwise size is shown in table 5 and in figure 37. (Mode 1.5 is simulated in a domain whose spanwise size is  $12\delta_{99}$ . Also, mode 1 is actually simulated in a domain whose spanwise size is  $16\delta_{99}$ . The spanwise resolution is comparable among all cases.)

For modes with  $k_z \leq 3k_z^0$ , an increase in the spanwise wavenumber delays transition. Meanwhile, for modes with  $k_z > 3k_z^0$ , a higher  $k_z$  promotes breakdown. We must be aware, however, that changing  $k_z$  affects the strength of the streaks (Zaki & Durbin 2005, 2006). The dependence of streak strength on the inflow  $k_z$  adds difficulties to distinguishing wavenumber effects from the influence of the disturbance amplitude.

The dependence of streak amplitude on  $k_z$  can be modelled by the coupling coefficient,  $\Theta$ , which was proposed by Zaki & Durbin (2005, 2006). The definition of  $\Theta$  includes the resonant term of the Squire response to O-S forcing, and also

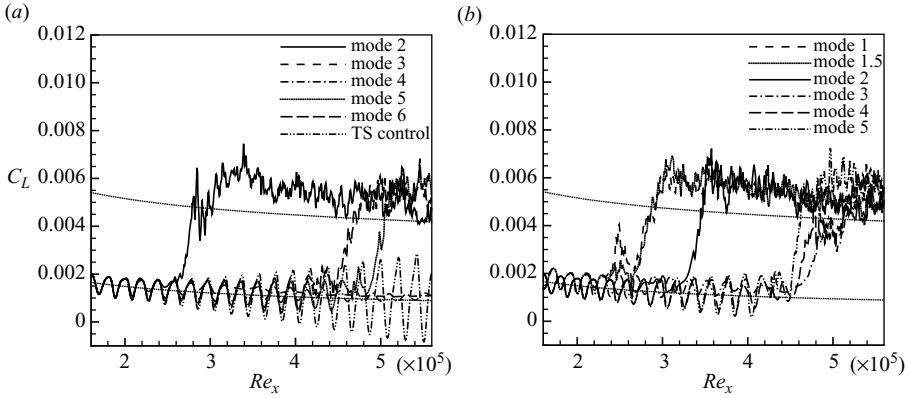


FIGURE 36. Effect of the spanwise wavenumber on transition location. Skin friction is plotted versus downstream Reynolds number. (a)  $A_{TS} = 1.0\%$ ,  $A_{con} = 2.1\%$ ; (b)  $A_{TS} = 1.0\%$ ,  $A_{con} = 1.0\%$ .

Case name	$A_{con}^0$ (%)	$A_{TS}^0$ (%)	$Re_t$	$k_z^\Delta$ ( $k_z^0$ )
Mode 1*	1.0	1.0	205 000	1.0
Mode 1.5*	1.0	1.0	222 000	1.5
Mode 2	1.0	1.0	244 000	2.0
Mode 2	2.1	1.0	214 000	2.0
Mode 2	3.0	1.0	206 500	2.0
Mode 3	1.0	1.0	445 000	3.0
Mode 4	1.0	1.0	404 000	2.0
Mode 5	1.0	1.0	400 000	1.25 ~ 1.67
Mode 5	2.1	1.0	427 000	1.25 ~ 1.67
Mode 5	3.0	1.0	509 000	1.25 ~ 1.67
Mode 6	2.1	1.0	386 000	1.2 ~ 1.5

TABLE 5. The dependence of  $Re_t$  on the spanwise wavenumber and the disturbance energy. Note: mode 1 and mode 1.5 are simulated in a wider computational domain with the same resolution.

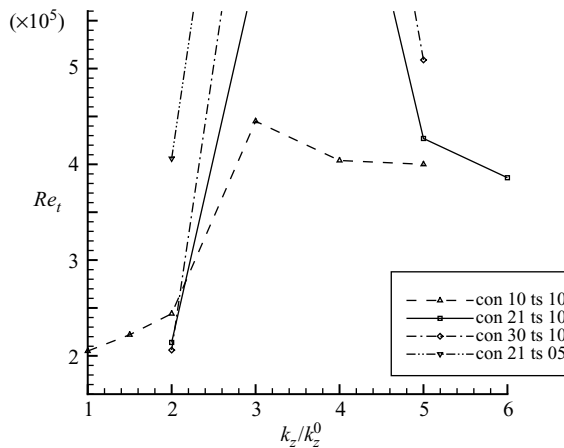


FIGURE 37. A graphical illustration of table 5. Decaying cases are treated by setting a large value to  $Re_t$ .

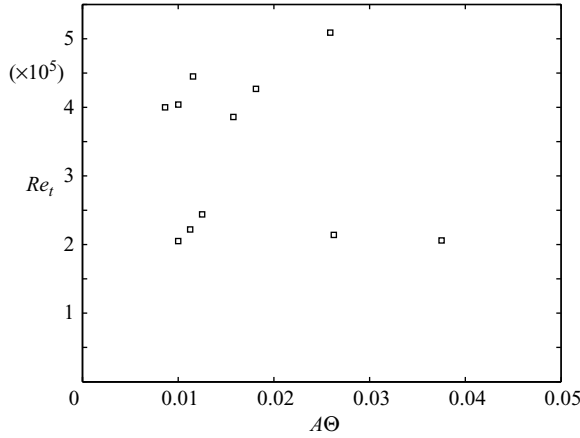


FIGURE 38. The transition Reynolds number vs.  $A^0_{con} \Theta$ .

accounts for the viscous decay rate of the continuous mode. If  $k_z$  affects transition solely through its influence on the streak amplitude, a direct correlation must exist between transition location and  $A^0_{con} \Theta$ . Figure 38 shows that such a correlation does not exist. Therefore, the role of the spanwise wavenumber of the continuous mode on transition must extend beyond its influence on the streak amplitude.

The spanwise wavenumber of the  $\Lambda$ -structures was also recorded from the simulations and is shown in table 5. The value of  $k_z^\Lambda$  is initially locked into the spanwise wavenumber of the continuous mode, up to  $k_z/k_z^0 = 3$ . At larger  $k_z$  for the streaks, the locking ceases to exist. Instead, the spanwise wavenumber of the  $\Lambda$ -structures decreases, which is an indication of the detuned instability. The shift from mode-locked to detuned instability is consistent with the Floquet results discussed above.

Finally, we briefly consider the role of streak unsteadiness on the boundary-layer stability. Our Floquet analysis is consistent with Cossu & Brandt (2004) who showed that steady streaks reduce the growth rate of primary T-S waves. Our simulations, as well as those by Fasel (2002), demonstrate that unsteady streaks, too, reduce the growth rate of the primary T-S waves.

The role of unsteadiness is more curious when considering the secondary instability due to the interaction of the streaks and TS waves. Fransson *et al.* (2005, 2006) studied this interaction for steady streaks and demonstrated that the presence of streaks is always stabilizing and suppresses transition. Our simulations, however, show that unsteady streaks promote transition.

Whether the discrepancy can be attributed to the streak unsteadiness was investigated using DNS. The new simulations preserved the inlet disturbance profile, but the continuous modes were assumed steady by setting  $\omega_{OS} = 0$ . The results for mode 5 with  $A^0_{TS} = 1.0\%$  and  $A^0_{con} = 2.1\%$  are shown in figure 39. The steady streaks completely suppress T-S waves and stabilize the flow. Therefore, the unsteadiness of streaks is significant in promoting breakdown.

In summary, our hypothesis to explain the DNS results is that two mechanisms are involved simultaneously. On one hand, the streaks suppress the growth rate of the primary T-S waves; on the other hand, the streaks trigger secondary instability of T-S waves. The competition of these two mechanisms causes the complicated behaviours found in our parameter studies. Mode 2 is probably an example of the dominance

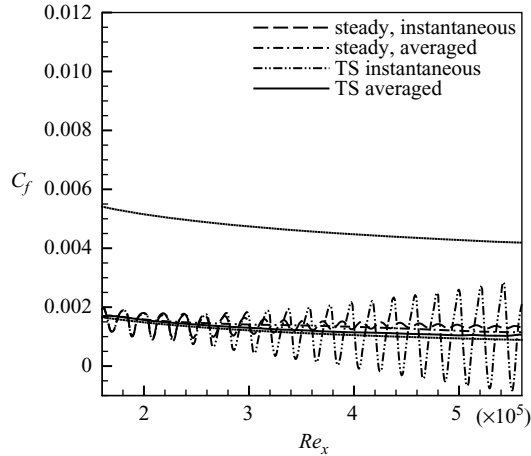


FIGURE 39. The skin friction curves for cases with steady and unsteady streaks, mode 5,  $A_{TS}^0 = 1.0\%$ ,  $A_{con}^0 = 2.1\%$ .

of secondary instability. The spanwise width of  $\Lambda$ -structures is therefore a result of secondary instability.

In mode 5, there is a range where secondary instability dominates; however, it requires a large T-S amplitude to occur. Because the streaks reduce the T-S growth rate, larger streak amplitudes might prevent T-S waves from reaching the amplitude required for secondary instability. That may be why the DNS shows that transition is delayed by large continuous mode amplitude and promoted at intermediate amplitudes.

Were the inflow disturbance a sum of modes – or a spectrum of free-stream turbulence – the boundary-layer response would be more complex than that studied herein. We would expect a combination of mode 2 type resonant secondary instability, and mode 5 type detuned instability. The present results provide a foundation for studying more complex inflow disturbances.

#### REFERENCES

- ABU-GHANNAM, B. J. & SHAW, R. 1980 Natural transition of boundary layers: the effects of turbulence, pressure gradient, and flow history. *J. Mech. Engng Sci.* **22**, 213–228.
- ANDERSSON, P., BERGGREN, M. & HENNINGSON, D. S. 1999 Optimal disturbances and bypass transition in boundary layers. *Phys. Fluids* **11** (1), 134–150.
- BERTOLOTTI, F. P., HERBERT, TH. & SPALART, P. R. 1992 Linear and nonlinear stability of the Blasius boundary layer. *J. Fluid Mech.* **242**, 441–474.
- BOIKO, A. V., WESTIN, K. J. A., KLINGMANN, B. G. B., KOZLOV, V. V. & ALFREDSSON, P. H. 1994 Experiments in a boundary layer subjected to free stream turbulence. Part 2. The role of TS-waves in the transition process. *J. Fluid Mech.* **281**, 219–245.
- BUTLER, K. M. & FARRELL, B. F. 1992 Three-dimensional optimal perturbations in viscous flow. *Phys. Fluids* **4** (8), 1637–1650.
- COSSU, C. & BRANDT, L. 2004 On Tollmien–Schlichting-like waves in streaky boundary layers. *Eur. J. Mech. B/Fluids* **23**, 815–833.
- FASEL, H. F. 2002 Numerical investigation of the interaction of the Klebanoff-mode with a Tollmien–Schlichting wave. *J. Fluid Mech.* **450**, 1–33.
- FRANSSON, J., BRANDT, L., TALAMELLI, A. & COSSU, C. 2005 Experimental study of the stabilization of Tollmien–Schlichting waves by finite amplitude streaks. *Phys. Fluids* **5**, 1–15.

- FRANSSON, J., TALAMELLI, A., BRANDT, L. & COSSU, C. 2006 Delaying transition to turbulence by a passive mechanism. *Phys. Rev. Lett.* **96**, 064501–4.
- GOSTELOW, J. P., BLUNDEN, A. R. & WALKER, G. J. 1994 Effects of free-stream turbulence and adverse pressure gradients on boundary layer transition. *J. Turbomachinery* **116**, 392404.
- HERBERT, T. 1983 Secondary instability of plane channel flow to subharmonic three-dimensional disturbances. *Phys. Fluids* **26**, 871–874.
- HERBERT, T. 1988 Secondary instability of boundary layers. *Annu. Rev. Fluid Mech.* **20**, 487–526.
- HUNT, J. C. R. & DURBIN, P. A. 1999 Perturbed vortical layers and shear sheltering. *Fluid Dyn. Res.* **24**, 375–404.
- HUGHES, J. D. & WALKER, G. J. 2001 Natural transition phenomena on an axial flow compressor blade. *J. Turbomachinery* **123**, 392–401.
- JACOBS, R. G. 2000 Bypass transition phenomena studied by computer simulation. PhD thesis, Stanford University.
- JACOBS, R. G. & DURBIN, P. A. 2000 Simulations of bypass transition. *J. Fluid Mech.* **428**, 185–212.
- KENDALL, J. M. 1985 Experimental study of disturbances produced in a pre-transitional laminar boundary layer by weak free stream turbulence. *AIAA Paper* 85-1695.
- KENDALL, J. M. 1991 Studies on laminar boundary layer receptivity to free stream turbulence near a leading edge. In *Boundary Layer Stability and Transition to Turbulence* (ed. H. L. Reed & R. Kobayashi). ASME-FED **114**, 2330.
- KENDALL, J. M. 1998 Experiments on boundary-layer receptivity to freestream turbulence. *AIAA* 98-0530.
- KLEBANOFF, P. S., TIDSTROM, K. D. & SARGENT, L. M. 1962 The three-dimensional nature of boundary layer instability. *J. Fluid Mech.* **12**, 1–24.
- KLEISER, L. & ZANG, T. A. 1991 Numerical simulation of transition in wall-bounded shear flows. *Ann. Rev. Fluid Mech.* **23**, 495–537.
- LIU, Y. 2007 Transition to turbulence by mode interaction. PhD thesis, Stanford University.
- LUCHINI, P. 2000 Reynolds-number-independent instability of the boundary layer over a flat surface: optimal perturbations. *J. Fluid Mech.* **404**, 289–309.
- MATSUBARA, M. & ALFREDSSON, P. 2001 Disturbance growth in boundary layers subjected to free-stream turbulence. *J. Fluid Mech.* **430**, 149–168.
- NAGARAJAN, S., LELE, S. & FERZIGER, J. 2007 Leading edge effects in bypass transition. *J. Fluid Mech.* **572**, 471–504.
- PHILLIPS, O. M. 1969 Shear-flow turbulence. *Annu. Rev. Fluid Mech.* **1**, 245–264.
- ROSENFELD, M., KWAK, D. & VINOKUR, M. 1991 A fractional step solution method for the unsteady incompressible Navier–Stokes equations in generalized coordinate systems. *J. Comput. Phys.* **94**, 102–137.
- SALWEN, H. & GROSCH, C. E. 1981 The continuous spectrum of the Orr–Sommerfeld equation. Part 2. Eigenfunction expansions. *J. Fluid Mech.* **104**, 445–465.
- TAYLOR, G. I. 1936 Effect of turbulence on boundary layers. In *Collected Papers of G. I. Taylor* (ed. G. Batchelor). Cambridge University Press, 1971.
- TUMIN, A. 2003 Multimode decomposition of spatially growing perturbations in a two-dimensional boundary layer. *Phys. Fluids* **15** (9), 2525–2540.
- WESTIN, K. J. A., BOIKO, A. V., KLINGMANN, B. G. B., KOZLOV, V. V. & ALFREDSSON, P. H. 1994 Experiments in a boundary layer subjected to free stream turbulence. Part 1. Boundary layer structure and receptivity. *J. Fluid Mech.* **281**, 193–218.
- WU, X., JACOBS, R. G., HUNT, J. C. R. & DURBIN, P. A. 1999 Simulation of boundary layer transition induced by periodically passing wakes. *J. Fluid Mech.* **398**, 109–153.
- ZAKI, T. A. & DURBIN, P. A. 2005 Mode interaction and the bypass route to transition. *J. Fluid Mech.* **531**, 85–111.
- ZAKI, T. A. & DURBIN, P. A. 2006 Continuous mode transition and the effects of pressure gradient. *J. Fluid Mech.* **563**, 357–388.